JJEES

JJEES (2020) 11 (2): 126-145
ISSN 1995-6681

Jordan Journal of Earth and Environmental Sciences

Paleocene-Eocene Thermal Maximum Record of Northern Iraq: Multidisciplinary Indicators and an Environmental Scenario

Ahmed N. Al-Fattah[1], Ali I. Al-Juboury[1], Imad M. Ghafor[2]

[1]Geology Department, Mosul University, Mosul, Iraq
[2]Geology Department, Sulaimaniya University, Iraq

Received 20 October, 2019; Accepted 1 March 2020

Abstract

In order to trace the environmental response of the PETM record in northern Iraq, three outcropping sections are selected at Sinjar, Dohuk, and Shaqlawa areas which included the Aaliji and Kolosh Formations. Lithologically, the fresh lithological color change was a distinctive field feature of PETM lithosomes. Biostratigraphically, the Paleocene/Eocene boundary is assigned by foraminfera in the prepared study at the same locations. Sedimentologically, PETM evidences are extrapolated through petrography (high micritic matrix ratio, magnetosomes, appearance of green algae (Dasycladacean) and early dolomitization). Facies analysis results are supported by the minor sea level rise (third or fourth order cycle) at the earliest Eocene as a one of the PETM indications. Clay mineral assemblage variations of formations referred obviously to warm, arid-seasonal climate conditions, which are consistent with the climatic trend of the southeastern Tethys region.

Geochemically and by using various methods, evidences of stable isotopes values in both formations give important hints for PETM. X-ray fluorescence analyses as geochemical indices fixed and confirmed the PETM environmental conditions, particularly anoxic or euxinic state and the rate of siliciclastic influx or the terrestrial input. Total organic carbon (TOC) and calcium carbonate weight percent variations present other signs regarding productivity nature, organic carbon preservation, and lysocline response during the PETM.

Multi-geoindicators and the integrated relationship among them suggested that the northern Iraq region was affected by the PETM climatic environmental perturbation in the marine realm within an epicontinental foreland basin.

Keywords: PETM, Paleocene, Eocene, Multidisciplinary study, Iraq

1. Introduction

The Paleocene-Eocene Thermal Maximum (PETM) represents a major climatic excursion of global nature that took place about 55.9 Ma. Global temperatures increased by ~ 6°C during a few thousand years, and the PETM is estimated to be approximately (~170) k.y. in duration (Zachos et al.,1993; Röhl et al., 2007; Harding et al., 2011; Zeebe and Lourens, 2019). The (PETM) was a geologically brief, rapid, abrupt, intemperate episode of global warming representing a significant impact on both marine and terrestrial ecosystem and is marked by a global temperature rise (5-8 °C) associated with a prominent negative carbon isotope excursion (CIE) ($\delta^{13}C$) (Sluijs et al., 2007).

There were multiple events within the late Paleocene and early Eocene, which imply a unique and non-singular trigger causing or leading to the release of huge and catastrophic or chronic fluxes of amounts of isotopically light CO_2 and/or CH_4 into the exogenic (ocean-atmosphere) that generated perturbations in the carbon cycle (Sluijs et al., 2007; Zhang et al., 2019; Elling et al., 2019). There are many causes suggested for the PETM such as the release of marine gas hydrates, Igneous Province activity, Permafrost thawing, Bolide impact (Dickens et al., 1995; Kent et al. , 2003; Svensen et al., 2004; DeConto et al., 2012; Zeebe, 2013; Schaller et al., 2016; Jones et al., 2019). Although such causes of the PETM remain controversial (Hupp et al., 2019), Methane release from clathrates is currently the most agreed upon cause which explains the PETM event (Khozyem et al., 2014; Hupp et al., 2019).

Bowen et al. (2006) maintained that rapid and extreme changes in the earth system may be triggered by natural carbon cycle perturbation even at times of globally-warm climates and in an ice-free world, and the PETM phenomena was the obvious indicator of that perturbation. They mentioned that an array of changes in the atmosphere, geosphere, hydrosphere, and biosphere have been documented during the PETM.

To bridge a gap in information related to the Paleocene Eocene thermal maximum succession locally and regionally, the current work presents a comprehensive study of the PETM event in Iraq through dealing with various geo-indicators and submitting a conceptual environmental model of climatic evolution of this warming event in Iraq.

In order to trace the geological responses in detail of the Iraqi geological record, three outcrop sections are selected carefully to represent the northern part of Iraq in Sinjar, Dohuk, and Shaqlawa areas, which contain the Aaliji and Kolosh formations (Figure 1). During the Paleocene and Eocene epochs these areas were located as a part of Tethys marine environments realm between paleolatitude (25-30°) N, (Scheibner and Speijer, 2008).

The samples were analyzed by adopting a multidisciplinary approach as the recent mode in paleoclimatic recognition.

* Corresponding author e-mail: alialjubory@yahoo.com

This included traditional petrography and scanning electron microscopy (SEM), major and trace elements by X-ray fluorescence (XRF) geochemistry, accompanied by stable isotopic geochemistry and clay mineralogy using X-ray diffraction (XRD). The multidisciplinary approaches of sedimentology, chemostratigraphy and clay mineralogy show the realm of climatic and paleoenvironmental evolution during the PETM from northern Iraq.

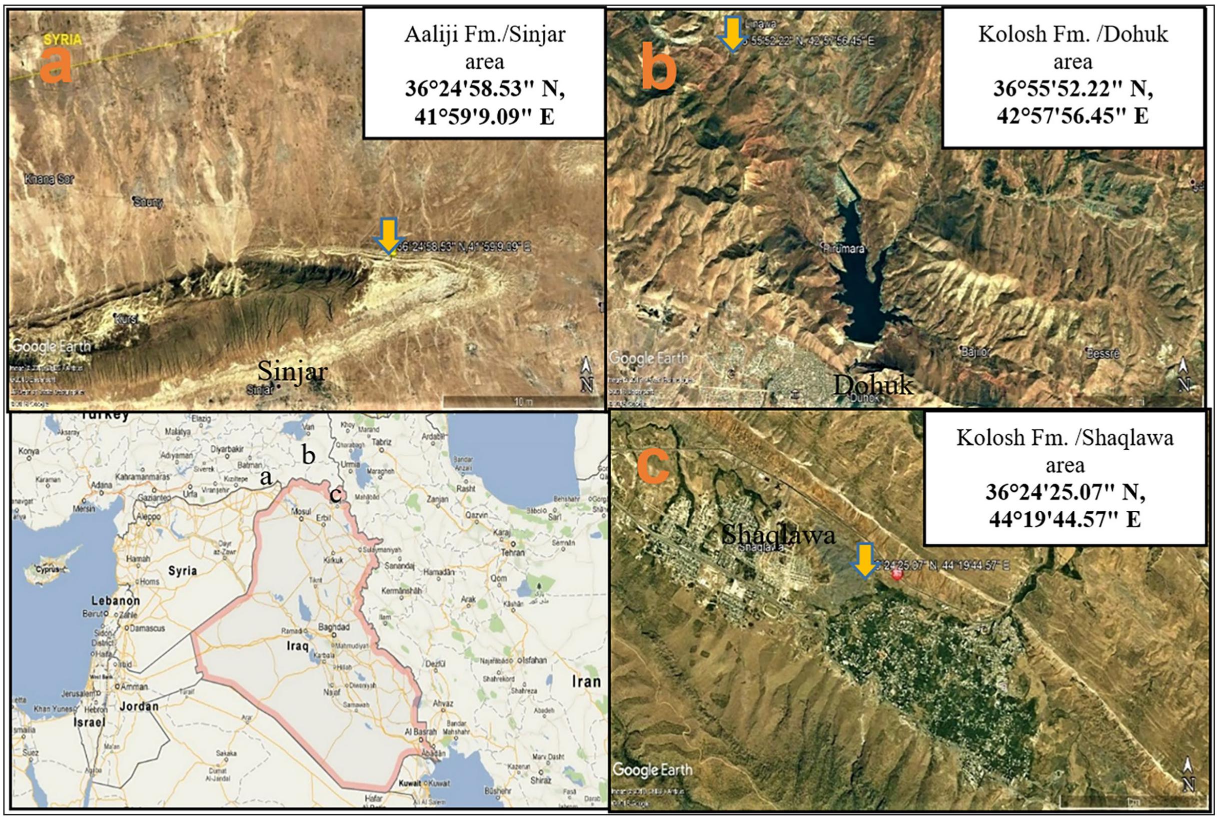

Figure 1. Location map of the studied areas.

2. Geological Setting

The middle Paleocene- Eocene megasequence (AP10) was deposited during a period of renewed subduction and volcanic activity associated with the final closure of the NeoTethys. The products of this subduction in Iraq are volcanics of the Walash Group (island arc setting) and the clastic-dominated Naopurdan Group (forearc setting) (Jassim and Buday, 2006).

During the Paleocene-Eocene period, Iraq was located between paleolatitudes 10-25° N (Sharland et al., 2001). These sediments were deposited in a NW-SE trending basin (70 km wide) in NE Iraq. This narrow basin extends longitudinally to Syria and Turkey, and SE Iran (Aqrawi et al., 2010). In the basin center and toward the Mesopotamian and Foothill Zones (Aaliji Formation) they were deposited in an offshore open marine or outer shelf basinal environments.

The Kolosh Formation, on the other hand, was deposited within narrow rapidly subsiding trough in marginal marine environments bordered to the NW-SE ridge by shallow water reef and lagoonal environments represented by Sinjar and Khurmala Formations in northern Iraq (Jassim and Buday, 2006).

The history of the early Paleogene continental shelf of most of Arabia is the reverse of much of the Mesozoic, with its extensive shallow-water (subtidal-supratidal) inner shelf carbonates (Umm Er Radhuma Formation), giving way to evaporites of lagoonal sabkha environments on a stable shelf (Rus Formation).The evaporates were replaced by carbonate-shelf conditions at about the turn of the lower to middle Eocene, when the beds of the (Dammam Formation) were deposited (Al-Sharhan and Nairn, 2003); Figure (2).

3. Materials and Methods

Field work and sampling have been achieved accurately in the outcrops; samples were measured and described lithologically. They were taken at least within 0.5 m intervals depending on bed thickness and lithological variations. Generally, the expected Paleocene- Eocene transition area of Aaliji and Kolosh Formations is distinguished in the field by thin and frequent limestone beds (5-25 cm) and/or black-gray high organic silty or marly shale beds, as well as yellowish, brownish, or a lighter rock color estimated in the early Eocene rocks.

3.1 Paleontological proxies

Analysis of foraminifera has been carried out firstly on three-five test samples located on a long interval space within the Paleocene/Eocene expected position for each section. The results enabled the resaerchers to constrain the upper Paleocene/lower Eocene spanning samples approximately. These samples exist between A15-A35 in Sinjar section (Aaliji Formation), D20-D35 in Dohuk section and Q15-Q35 in Shaqlawa section (Kolosh Formation), see Figures (3 A - C). Foraminifera were extracted from most of the indurated marl and limestone using the washing method (Brasier, 1980; Lirer, 2000).

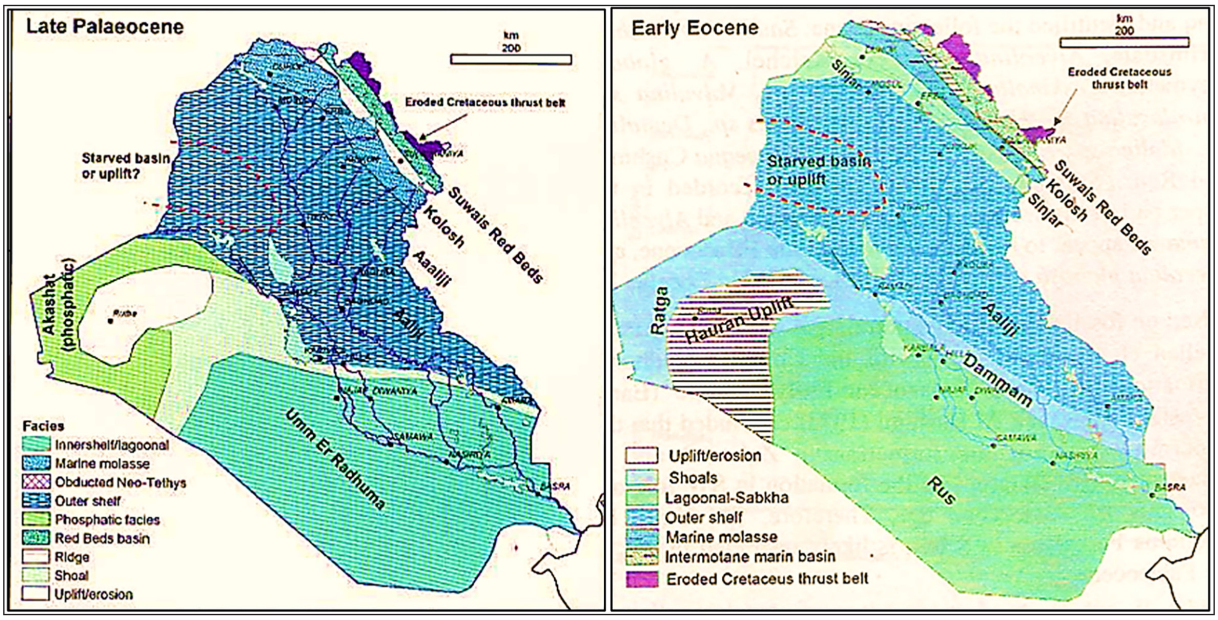

Figure 2. Late Paleocene –Early Eocene paleogeography and facies distribution of Iraq from Jassim and Buday (2006).

3.2 Mineralogical Proxies

Sixty thin sections were studied petrographically by the Vickers polarized microscope at the Earth Science Department, Royal Holloway, University of London.

SEM for identification and description of the clay mineral phases were carried out with magnifications between 100X and 16000X with gold-coated samples. Analysis was carried out at the scanning microscope unit of Royal Holloway, University of London using the Hitachi S-3000N scanning electron microscope.

A representative portion of each sample was manually ground to a fine powder using a ceramic mortar and pestle. The powder was packed into a recessed plastic holder and preferred orientation was minimized. The samples were analyzed using a Philips X-ray diffractometer (PW3710) scanning from 4º to 40º 2θ. Peak identification was enabled using PDF/ICCD database and quantification was done through Rietveld analysis using commercial software program Siroquant (Sietronics, Australia). Analysis was done at laboratories of the Department of Earth Sciences, Royal Holloway, University of London.

3.3 Geochemical proxies

X-ray fluorescence analysis of the major and trace-element geochemistry of the selected samples was performed (using AXIOS spectrophotometer made by PANalytical) at the laboratories of the Department of Earth Sciences, Royal Holloway, London University. Sample preparation includes two steps; fused glass disc and pressed pellets preparations. Pellets are then dried in an oven overnight at 80˚C before being analyzed.

For carbon and oxygen isotope measurements of bulk carbonate samples, ~300 to 1000 µg of the powdered samples (obtained by drilling fresh rock surfaces or of the samples crushed with a pestle and mortar) were first roasted in a vacuum oven for one hour at 200˚C to drive off residual water and volatiles. For carbon- and oxygen-isotope measurements of foraminifera, ~100 to 300 µg of foraminifera were picked and cleaned with methanol before being oven dried at 70˚C. Foram tests were then crushed using a glass rod. All samples were analyzed by continuous-flow mass spectrometry using a Gas bench connected to a Thermo-Finnegan Delta +XP mass spectrometer. All isotope data were measured in the Bloomsbury Environmental Isotope Facility (BEIF) at the University College London and were reported in ‰ deviation from Vienna Peedee belemnite (PDB). One standard deviation error on internal standards was better than ±0.1‰ for both $\delta^{13}C$ and $\delta^{18}O$ during the analysis of the samples.

Bulk rock samples were analyzed for their Total Organic Carbon (TOC) and $CaCO_3$ contents. Samples for (TOC) analyses were crushed to a fine powder, then weighed (~60 to 100 mg) and decarbonated with ~10% HCl in silver foil cups. Once decarbonation was complete, the samples were left to dry. The samples were weighed (~10 to 30 mg) in tin cups for Total Carbon (TC) analysis. All samples were analyzed by combustion in a Thermo Finnegan Flash Elemental Analyzer (EA). Reproducibility of an internal standard was better than 0.1 wt. %. $CaCO_3$% was calculated by subtracting TOC from TC, multiplying it by 8.33333 (recurring). All analyses were achieved at the University College London (UCL), UK.

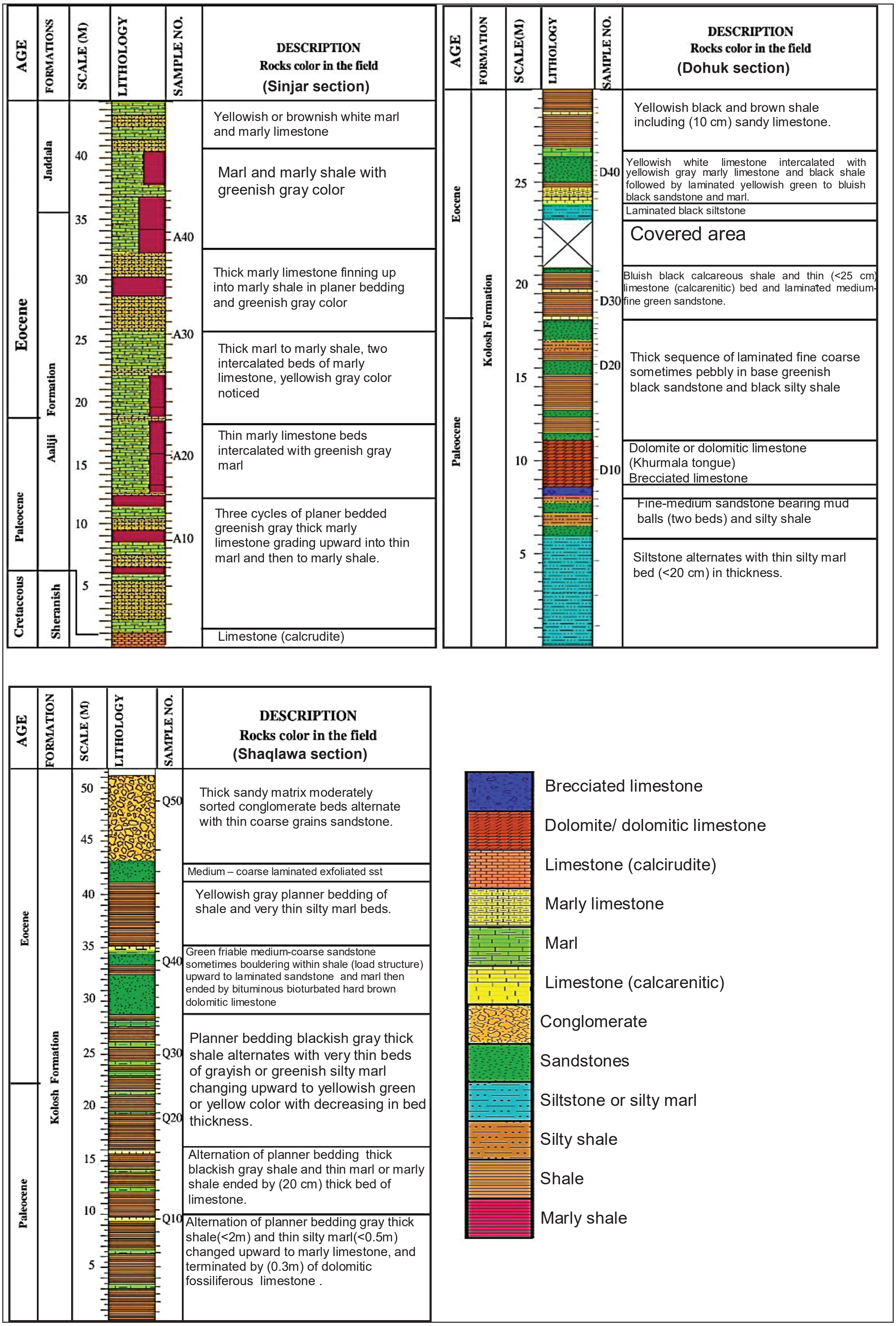

Figure 3. Lithostratigraphy and age assignment of Aaliji Formation and Kolosh Formation at Dohuk and Shaqlawa area.

4. Results

4.1 Lithostratigraphy

The expected Paleocene-Eocene transition area of the Aaliji and Kolosh formations is distinguished in the field by thin and frequent limestone beds (5-25 cm) and/or black-gray high organic silty or marly shale beds, as well as yellowish, brownish, or lighter rock color estimated in the early Eocene rocks.

In the Aaliji Formation, the studied succession is composed mostly of marly limestone, marlstone, and calcareous shale. The Paleocene interval is mostly made up of thinning upward marly limestone beds associated with thickening upward marlstone and calcareous/marly shale. At the upper Paleocene-lower Eocene lithesome, the intercalation of the thin-bedded calciturbidites the marly limestone (4-10 cm thickness) beds become more frequent, interestingly accompanied by color change from greenish-gray dominated facies to yellowish and /or brownish-gray dominated facies, Plate (1 A and B).

The Kolosh Formation (Dohuk and Shaqlawa sections) exhibit other field physical properties, which are considered as a clue to PETM lithosome. In the Dohuk section, an abrupt transition from clastic turbidite Bouma sequence mode deposits to calcarenitic tempestite sequence mode deposits (eventstone) attracts the attention. Also, there is an abnormal event particularly when the main sequence color changes from green to a yellowish white color in addition to the presence of shells (tempestite beds), Plate (1 C).

On the other side, yellowish marl and reddish brown bands as well as high organic- matter-rich black shales charecterize the PETM lithesome at Shaqlawa section (deep marine Kolosh facies), Plate (1 D).

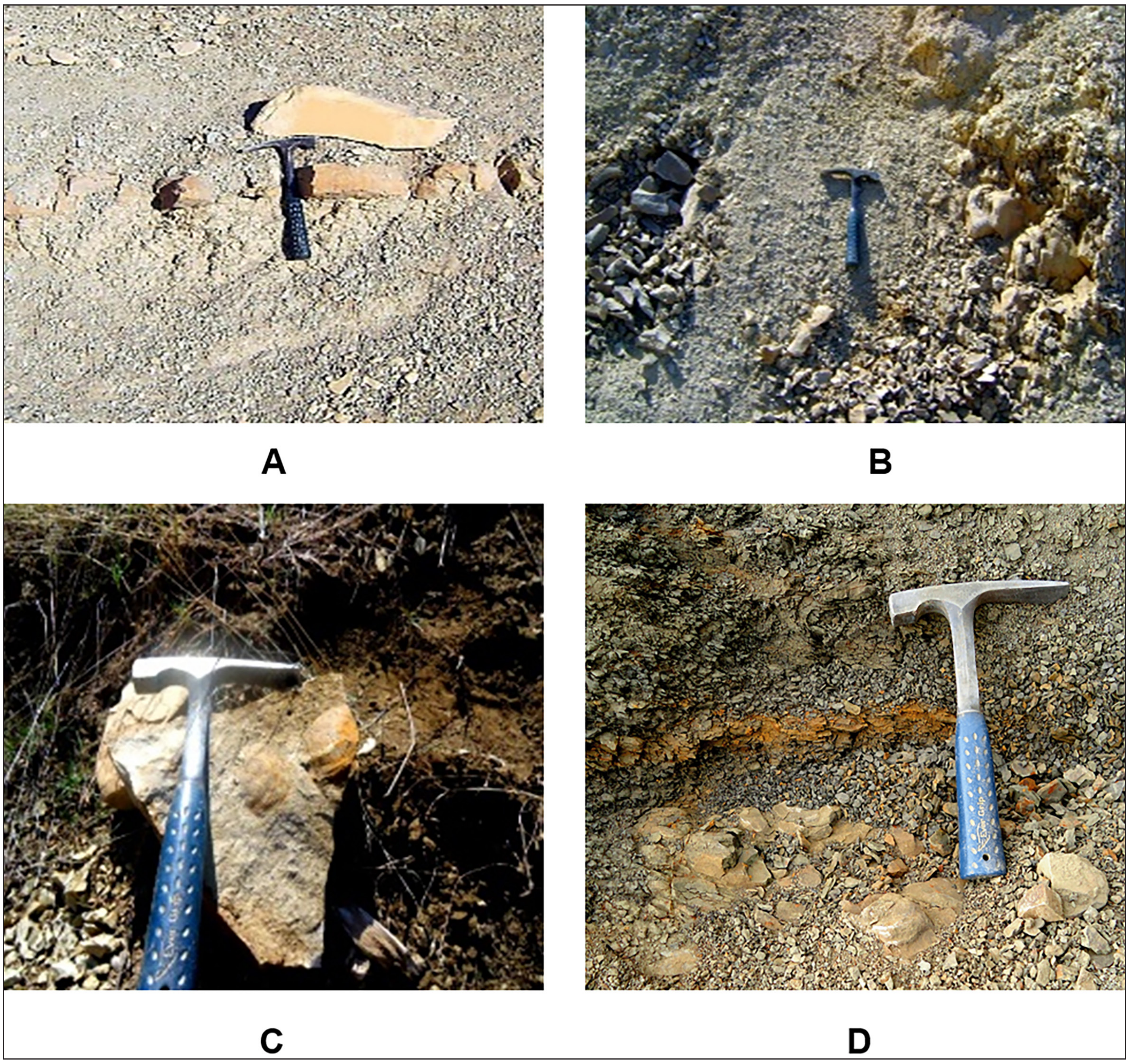

Plate 1. A. Calciturbidite thin beds of marly limestone, **B.** color defference at Paleocene-Eocene transition facies of Aaliji Formation at sinjar anticline. **C.** yellowish white calcarenitic limestone (Tempestite) in Dohuk section. **D.** yellowish marl and reddish brown band in the black shale of Shaqlawa section.

4.2 Biostratigraphy

Adopting Berggren and Pearson (2005), the Paleocene-Eocene biostratigraphic boundary of Aaliji Formation delimited at Last Appearance Datum (LAD) of Morozovella velascoensis (sample A23) and First Appearance Datum (FAD) of Acarinina sibaiyaensis (sample A24) Figure (3 A), (AL Fattah et al., in press).

In the Kolosh formation at Dohuk and Shaqlawa, the last recorded occurrence of Angulogavelinella avnimelechi in sample (D28) and sample (Q24) respectively close the uppermost Paleocene time, in turn the early Eocene time is characterized by deep-water agglutinated foraminifera (DWAF) assemblages that are recorded in samples (D31, Q25) Figure (3 B,C) (AL Fattah et al., in press).

Planktonic foraminifer's assemblages respond to PETM environmental conditions represented by species reorganization (decline, abundance) and morphological optimal adaptation (shape, size). While the benthic foraminifera respond was represented by the benthic extinction event (BFEE) (in deep locations) with a general decrease in the generic diversity of photoautotrophic (oligotrophic conditions) larger foraminifera followed by abundance stage (in shallow locations) (AL Fattah et al., in press).

4.3 Chemostratigraphy

Isotope composition ($\delta^{13}C$ and $\delta^{18}O$)

Carbon stable isotope values of bulk rock samples range from (- 1.09 ‰ to 0.65 ‰) in the Aaliji Formation with an average of (0.03 ‰) and a negative magnitude of the highest peak (about - 1.1 ‰) Figure (4 A). In turn, they range between (-6.99 ‰ to 0.64 ‰) with an average of (-2.24 ‰) and a negative magnitude of (-1‰ around Paleocene-Eocene boundary) in the Kolosh Formation (Dohuk section) Figure (4 B), and between (-37.01 ‰ to -1.81 ‰) with an average of (-10.13 ‰) and a negative magnitude of (-13‰ around Paleocene-Eocene boundary) in the Kolosh Formation (Shaqlawa section), Figure (4 C).

Although these results seem to be affected by diagenesis, particularly in the Kolosh Formation, distinctive hints observed for a negative excursion (CIE) in both Formations coincided with the early Eocene. These hints are main peaks, a negative trend line of values, abrupt shifting and magnitude of highest peak occur within the accepted (CIE) range of marine environments Figures (4 A - C).

The peak amplification may be a result of the reworking of depleted siliciclastics (Höntzsch et al., 2011) (Duhok) or the original signal of carbon isotope overprinted and accentuated by the early diagenetic dolomitization due to the bacterial sulfate reduction and/or more likely by the high organic-matter content (Bolle et al., 2000; Mazzullo, 2000) as (Shaqlawa) section.

The early Eocene peak magnitude values approximation between Kolosh (Dohuk) and Aaliji Formations confirmed confidently that those values are likely true especially at the Aaliji Formation because it is comprised of limestones and marls that have been indurated or compacted during the early diagenesis, and have a high ratio of calcite/organic matter; thereby they may represent closed systems with respect to carbon isotopes (retaining original signals) according to Schmitz et al. (1997).

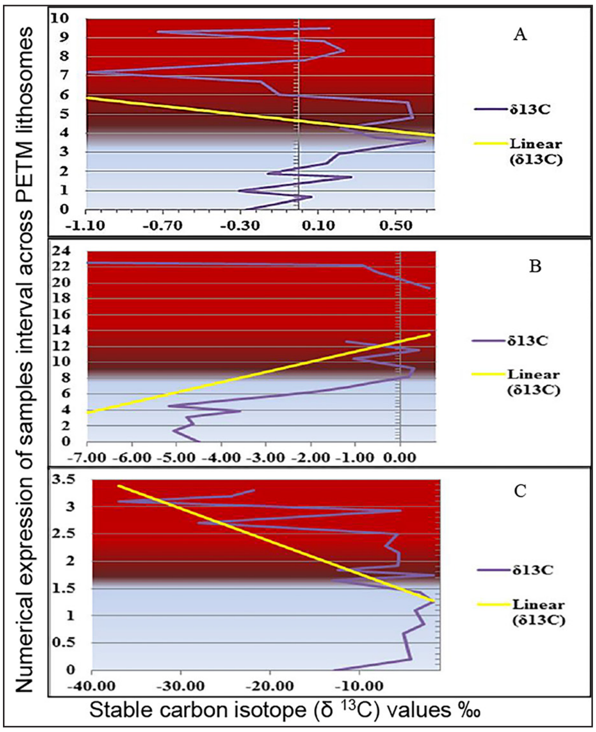

Figure 4. TStable carbon isotope ($\delta^{13}C$) behavior taken from bulk samples across PETM lithosomes of the studied sections, **A.** Aaliji Formation at Singar section **B.** Kolosh Formation at Dohuk section, **C.** Kolosh Formation at Shaqlawa section, the contact between two colors corresponds to the Paleocene / Eocene contact.

Isotopic analysis of $\delta^{13}C$ for the Aaliji Formation mixed planktonic foraminifera ranged between (0.8 ‰ and 1.4 ‰) and they are represented by two peaks after the Paleocene/ Eocene contact with a peak magnitude of less than (< 0.5 ‰). These positive values can be interpreted as a result of the recrystallization diagenetic process (dissolution and reprecipitation of calcite) on the foraminiferal tests, where the recrystallization causes "smoothing" of the original or bulk samples isotope signals (Veizer, 2009). However, the early Eocene shifts are observed inspite of a lesser magnitude, Figure (5 A).

Oxygen ($\delta^{18}O$) stable isotope is considered as a function to precipitation and temperature as well as salinity variations (Uchikawa and Zeebe, 2010). Foraminferal (mixed species) isotope analysis of $\delta^{18}O$ results for the Aaliji Formation showed values ranging between (-4.3 ‰ and -5.6 ‰) along with two peaks: a low magnitude peak at the Paleocene/ Eocene boundary and a high magnitude peak at early Eocene as well as a negative trend line and a peak magnitude of less than (<1 ‰), Figure (5 B). Bulk sample $\delta^{18}O$ values at the Aaliji Formation fluctuated between (-4.52‰ and -3.36‰) with an average of (-3.75‰). More than one negative peak was observed after the Paleocene/ Eocene boundary (within the early Eocene) with a peak magnitude of (<1‰), Figure (6 A). On the other hand, $\delta^{18}O$ values at the Kolosh Formation in Dohuk section fluctuated between (-5.19‰ and 0.19‰) with an average of (-3.58‰). After the Paleocene Eocene boundary, the samples start to tend towards negative values until they cease in the covered area which is expected to have values that are more negative (a high magnitude peak) Figure (6 B). In the Kolosh Formation and at the Shaqlawa section, $\delta^{18}O$ values fluctuated between (-7.31‰ and -3.79‰) with an average of (-5.54‰), high magnitude negative peaks were observed around the Paleocene/ Eocene boundary especially in the early Eocene, Figure (6 C).

Despite the role of diagenesis affecting the original $\delta^{18}O$ signal, observed distinctive hints support the partial preservation of the original $\delta\ ^{18}O$ signal suggestion in both of the Aaliji and Kolosh formations. Thus, the general trend of the original $\delta^{18}O$ signal remains preserved particularly in the Aaliji Formation, whereas in the Kolosh Formation, it is expected to be vulnerable to post depositional processes due to a relatively shallow marine environment Figure (5, B) and (6). Briefly, the original $\delta^{18}O$ signal in the Aaliji Formation may be less modified by diagenesis and more preserve than in the Kolosh Formation.

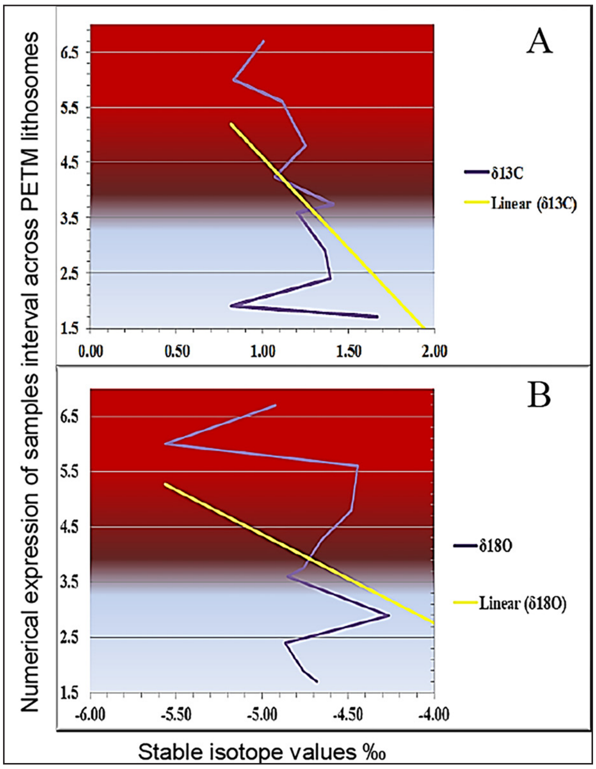

Figure 5. Planktonic foraminifera (mixed species) stable isotope behavior taken across PETM lithosome of Aaliji Formation. **A.** ($\delta^{13}C$) and **B.** ($\delta^{18}O$), the contact between two colors correspond to the Paleocene / Eocene contact.

5. ???????

5.1 Major and Trace-Element Analysis

It is clear that the elemental geochemistry of the PETM Lithosomes at the Aaliji and Kolosh (Shaqlawa section) formations is partly controlled by a bulk mineralogical composition. The dominated clay mineral amount and TOC concentration in the deposits (discussed later) appear to be largely the two major controls on the absolute abundance of many of the elements (Soliman et al., 2011).

In the Aaliji Formation, with the exception of CaO, MnO, P_2O_5, Na_2O, and SO_3, the other major elements oxides increased in the early Eocene and are represented in two phases separated by anomalous values in sample (A27) which is composed of marly limestone. The increased phases coincided with marly shale lithologies as shown in Figure (7). These major element features suggested a slight increase in contribution from detrital materials.

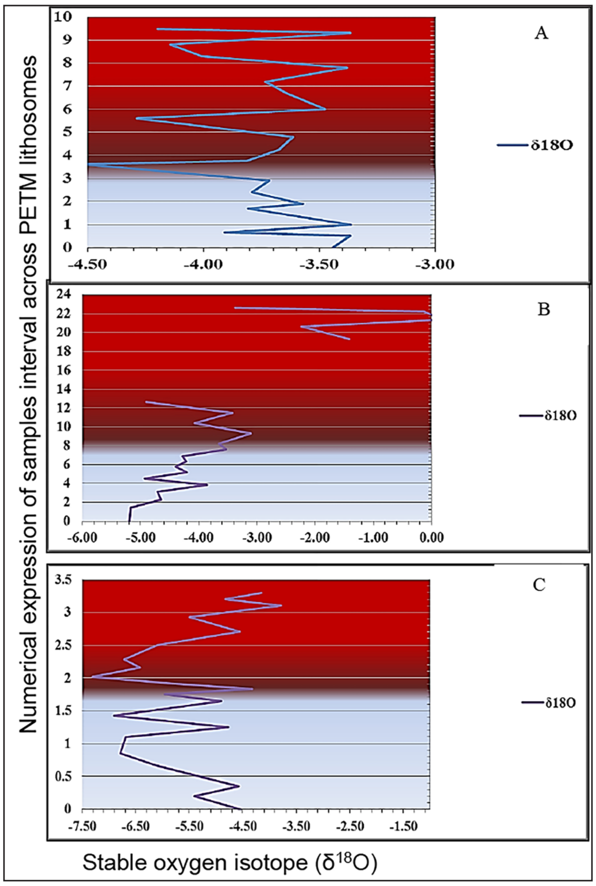

Figure 6. Stable oxygen isotope ($\delta^{18}O$) behavior taken from bulk samples across PETM lithosomes of studied sections. **A.** Aaliji Formation. **B.** Kolosh Formation at Dohuk section. **C.** Kolosh Formation at Shaqlawa section, the contact between two colors correspond to Paleocene / Eocene contact.

The following geochemical indices (Mo/U, Mo/Cr, V/Al, V/Cr, Ni/Co, U/Th, V/V+Ni, Fe/Ti, U/Al, Mo/Al, Si/Al, K/Al, Zr/Al, Rb/Al) are increased, while other indices as (Ti/Al, Mn/Al, Ba/Al, Ni/Al, Mg/Al, Fe/Al) are decreased Figure (8).

These results are interpreted as follows: the variations in paleoredox sensitive indicator ratios increase in (Mo/U, Mo/Cr, V/Al, V/Cr, Ni/Co, U/Th, V/V+Ni, Fe/Ti, U/Al and Mo/Al) and decrease in Mn/Al indicate deposition under anoxic or euxinia conditions (Giusberti et al., 2007; Sluijs et al., 2008 ; Giusberti et al., 2009; Alegret et al., 2010; Schulte et al., 2011a; Dickson et al., 2012; Liu et al., 2012). Similarly, the increase in terrestrial input indicators including (Si/Al, K/Al, Zr/Al, Rb/Al) are recorded. The Si/Al peak is rather related to the high abundance of quartz concurrent with a low level of phyllosilicate abundance reflecting a decrease in the flux of Al (relative to Si); the increased Si/Al ratio is best explained by a relative increase of fine-grained silt-sized quartz. Such a marked increase in the Si/Al ratio and quartz content can reflect significant arid climatic conditions (Schulte et al., 2011a). The overall inverse relationship of K/Al with $CaCO_3$ is a strong evidence of its detrital source and corresponds well with the relatively higher input of illite (K-rich) by fluvial or aeolian transport (Thomas and Bralower, 2005). The zirconium- and titanium-bearing heavy minerals (e.g., rutile, ilmenite, sphene, and zircon) are generally enriched in sandsilt-sized siliciclastic detritus and Al is generally enriched in the clay-size fraction (Fralick and

Kronberg, 1997 and Dypvik and Harris, 2001 in Schulte et al., 2011a). Thus, it is obvious that the high Zr/Al, and Rb/Al ratios as well as the K/Al, ratio document a brief influx of more detrital sediments and suggest that the provenance area was tapped during the rapid sea-level rise (Schulte et al., 2011a; Ver Straeten et al., 2011). Because of the strong resistance of Ti and Al to diagenetic alteration, the Ti/Al ratio has been used as a useful proxy for the occurrence of extraneous material in sedimentary sequences (Lipinski et al., 2003; Schmitz et al., 2004 in Soliman et al., 2011). Likely, this explains the decrease in Ti/Al ratio in the Aaliji Formation. This is attributed to a relative rarity or absence of extraneous material (basinal environments). Low Ti/Al values may coincide with sapropel beds and reflect reduction in the aeolian dust supply (Ver Straeten et al., 2011; Liu et al., 2012). A sharp decline in the Ba/Al ratio that is used as a proxy for biological productivity suggests sharp transition from a eutrophic to an oligotrophic or mesotrophic condition at the early Eocene that is concomitant with the foramineferal evidence. Fe/Al and Ni/Al ratios showed that the strength of sulphate-reducing (i.e. sulphidic) conditions was relatively small (Liu et al., 2012). Finally, the slight decrease in the Mg/Al ratio and its subsequent increase is attributable to the brief dissolution period of the syndepositional dolomite because of CCD shallowing.

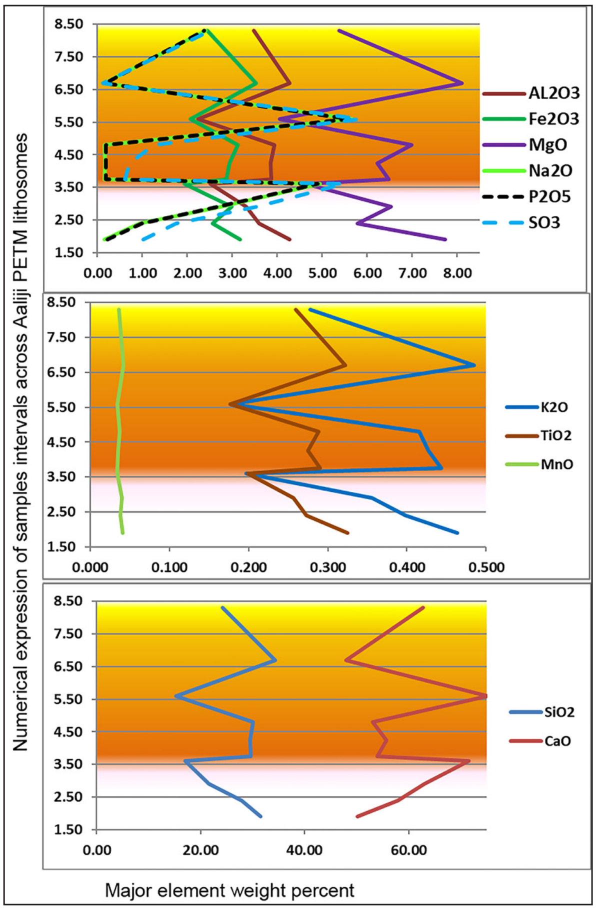

Figure 7. Major elements' behavior across the Aaliji Formation PETM lithosome,the contact between two colors correspond to the Paleocene / Eocene contact.

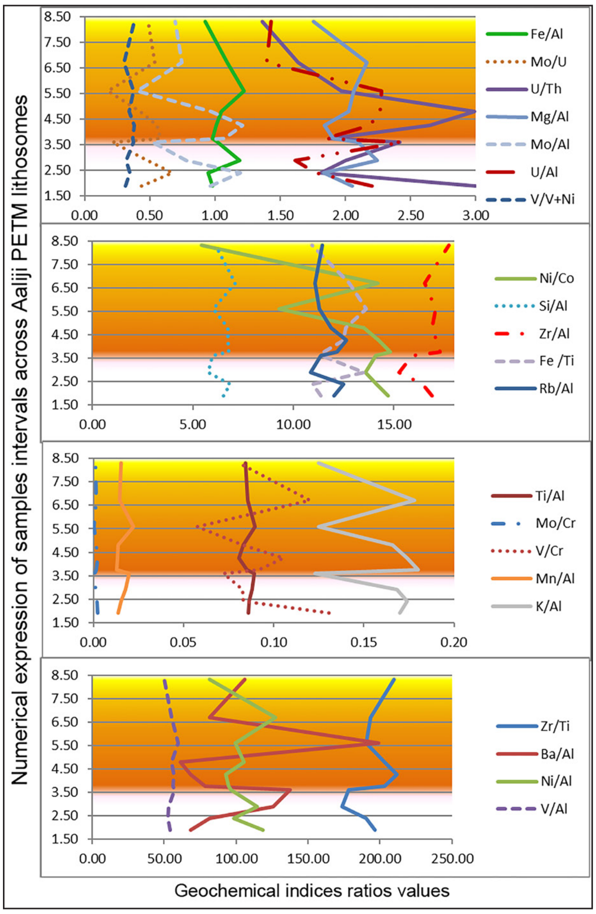

Figure 8. Geochemical indices ratios variations across Aaliji formation PETM lithesome, the contact between two colors correspond to Paleocene / Eocene contact.

In the Kolosh Formation (Shaqlawa), although oscillations in major elements and oxide values are attributed to the alternation of silty marl beds with shale, there are relative increasing trends in all oxides with the exception of CaO and MnO around and after the Paleocene/Eocene boundary Figure (9). This increase is interpretable in shale as a contribution of detrital clay minerals, whereas it may reflect the occurrence of a high silt ratio in silty marl beds after the Paleocen /Eocene boundary.

The geochemical elemental ratios such as (V/Al, Ni/Co, Fe/Ti, Zr/Ti, Mg/Al, Si/Al, Zr/Al, Mn/Al, and Ni/Al), CaO and MnO oxides were low, whereas (Ti/Al, Ba/Al, Fe/Al, K/Al, Mo/Al, U/Al, Mo/U, Mo/Cr, V/Cr, U/Th, V/V+Ni and Rb/Al) ratios were high, Figure (10).

The increase in paleoredox sensitive indicator ratios (Mo/U, Mo/Cr, V/Cr, U/Th, V/V+Ni, U/Al and Mo/Al) as well as the decrease in Mn/Al may be referred to depleted-oxygen (dysoxia or anoxia) environmental conditions. Other paleoredox sensitive indicator ratios that are decreased abnormally (V/Al, Ni/Co, and Fe/Ti) are attributed to the ventilation style which is lower than that in the Aaliji section as evidenced by the low V/Al ratio. In addition, the decrease in Ni/Co ratio is negligible since its value is still above seven (Alegret et al., 2010), whereas a slight decrease in Fe/Ti may interpreted by the high siliciclastic flux at the Kolosh Formation compared with the Aaliji Formation which is consistent with absence of iron scavenging period from a euxinic water column to form syngenetic pyrite (Schulte et al., 2011a). The terrestrial input indicators (Si/Al, K/Al, Zr/Al, Rb/Al) exhibit an increase in K/Al, Rb/Al and a decrease in Si/Al and Zr/Al ratios. The increased values are interpreted as a reflection of more detrital influx of sediments and mineral phases (largely illite) and during sea level rise conditions (Schulte et al., 2011a). The Zr/Al ratio decrease may be a function of the diminishing sand-sized fractions in the Kolosh clastic sediments (Ver Straeten et al., 2011). A drop in the Si/Al ratio at the onset of the PETM points can be attributed to either the reduced Si input derived from silicic organisms (e.g., radiolarians) or the lowered input of (aeolian?) quartz (Schulte et al., 2011b). Since Ti/Al ratio is used as a useful proxy for the occurrence of extraneous material in sedimentary sequences, its slight high value indicates the occurrence of more extraneous material, and this coordinated with clastic nature of Kolosh Formation. Increase in the Fe/Al ratio can be referred to the strength of sulphate-reducing conditions or may indicate a more intense weathering (Sluijs et al., 2008; Liu et al., 2012). The Ba/Al ratio showed an increased value suggesting prevailed eutrophic conditions with some fluctuations which might be attributed to mesotrophic conditions.

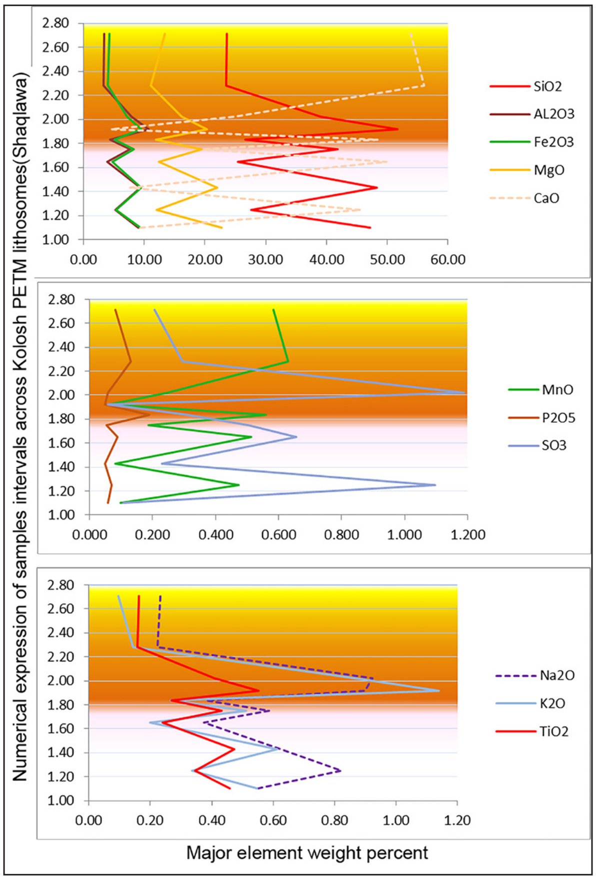

Figure 9. Major elements' behavior across the Kolosh Formation PETM lithesome (Shaqlawa section), the contact between two colors correspond to the Paleocene / Eocene contact.

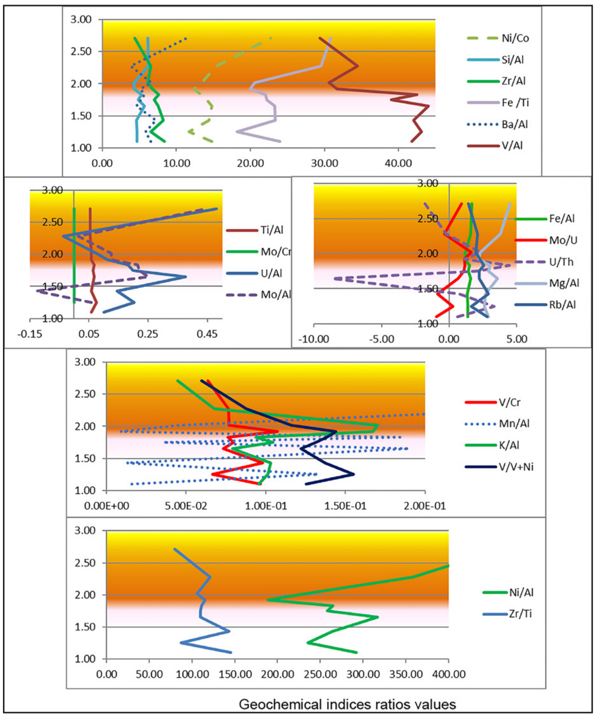

Figure 10. Geochemical indices ratio variations across the Kolosh Formation PETM lithesome (Shaqlawa section), vertical axis represents samples' intervals of PETM lithesome, the contact between two colors correspond to the Paleocene / Eocene contact.

5.2 Total Organic Carbon (TOC)

Total organic carbon ratios of the bulk rock samples range from 0.19 % to 1.14 % with an average of 0.66 at the Aaliji Formation. They range from 0.0496 % to 0.62 % with an average of 0.22 % at the Kolosh Formation (Duhok section), and from 0.058 % to 0.601 % and average of 0.22 % at Kolosh Formation (Shaqlawa) along the PETM lithosomes.

The similarity in average values between the Duhok and Shaqlawa sections supports the idea of a similar source at the Kolosh Formation in these sections. The TOC amounts are high at the early Eocene in all studied sections, and can be related in principle to low sedimentation rates (Aaliji Formation) and/or siliciclastic input materials (terrestrial source of organic matter), and \or elevated organic-matter production. Figure (11).

In general, the change in TOC contents suggests that there was a profound change in the conditions (Meadows, 2008). In many of the continental shelf and epicontinental sections that span the PETM (as the studied sections), total organic carbon (TOC) is high (Cohen et al., 2007).

The increase of organic fluxes to the sea, the increase of primary productivity, and the improved preservation under anoxia conditions (lack of bioturbation) are together probable causes of the TOC enrichment during PETM. (Tremolada and Bralower, 2004; Ernst et al., 2006; Sluijs et al., 2008; Meadows, 2008; Soliman et al., 2011).

Moreover, TOC enrichment in shelf/epicontinental sea settings is considered as an evidence for the transient sea level rise (Arthur and Sageman, 2004). Elements that bond to organic matter or form sulfide compounds are enriched in strata under low dysoxic to anoxic conditions. Briefly, the paleoredox sensitive indicator ratios that suggest deposition under anoxic conditions appear to be linked to the enhanced TOC values and the very finely laminated shales (no bioturbation) and the transient sea level rise at the PETM lithosomes in the studied sections.

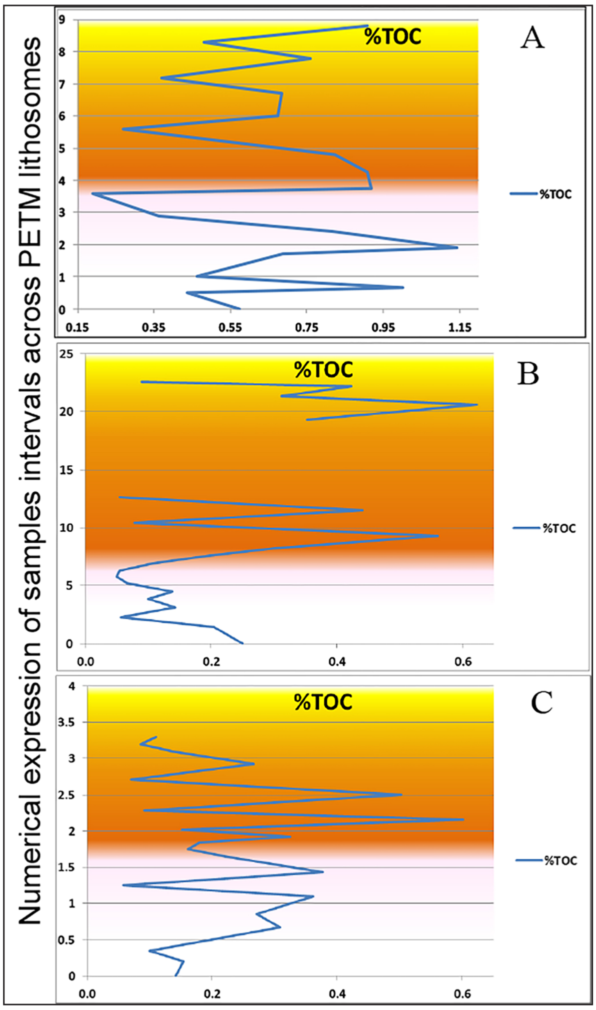

Figure 11. Total organic carbon percentage variations across the PETM lithosomes. **A.** Aaliji Formation. **B.** Kolosh Formation at Dohuk section. **C.** Kolosh Formation at the Shaqlawa section, the contact between two colors correspond to the Paleocene / Eocene contact.

5.3 Calcium Carbonate Ratios

Calcium carbonate ratios fluctuated between 60.74% and 84.31% in an average of 70.04 % at the Aaliji Formation. At Kolosh Formation (Dohuk section), they ranged from, 9.82% to 81.33% with an average of 50.8% and from 5.25% to 67.7% with an average of 37.4% at the Kolosh Formation (Shaqlawa). $CaCO_3$ weight percentage values begin to decline relatively after the base of Eocene at all sections except Dohuk, but they returns to improve upwards Figure (12). This exception may be attributed to the dissolution contrast between deep sea and shelf deposits, where shelf deposits were largely unaffected by dissolution that is originated from the lysocline shallowing during PETM (Zachos et al., 2005; John et al., 2008).

The decrease in $CaCO_3$ accumulation/preservation rates during the PETM was driven primarily by a significant increase in sea floor dissolution, rather than by a major decrease in surface water biological production, or is rather related to siliciclastic dilution (Nicolo et al., 2007; Nguyen et al., 2009). Moreover, the $CaCO_3$-poor sediments are enriched in redox-sensitive trace metals such as Mo, U and V that are indicative of bottom water anoxia, accompanied by increases in TOC and may include surface of maximum flooding (MFS) (Sluijs et al., 2008; Ver Straeten et al., 2011).

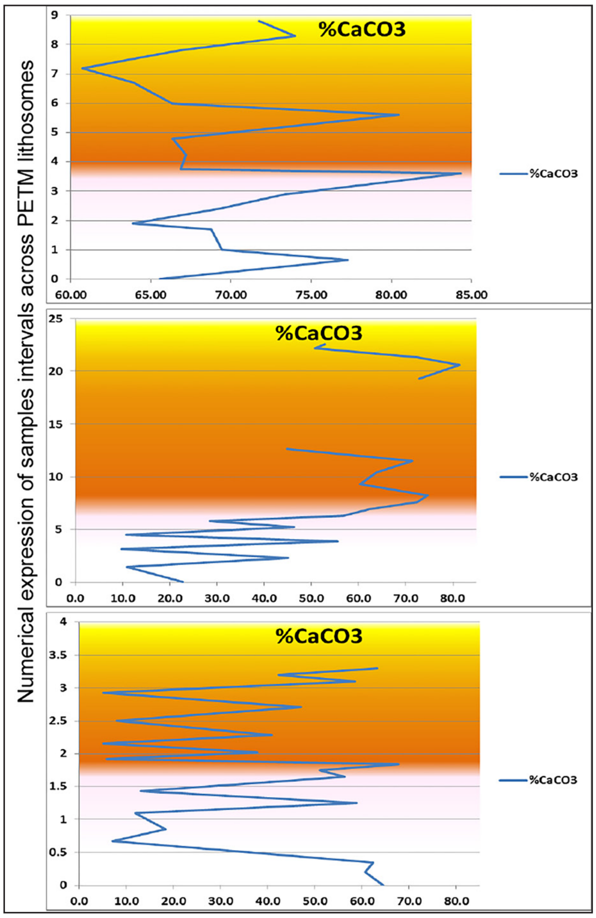

Figure 12. Calcium carbonate ratio variations across the PETM lithosomes. **A.** Aaliji Formation. **B.** Kolosh Formation at Dohuk section. **C.** Kolosh Formation at Shaqlawa section, the contact between two colors correspond to the Paleocene / Eocene contact.

6. Sedimentology

6.1 Petrography and Facies Analysis

PETM facies (facies or lithosome spanning or nearly equivalent to the uppermost Paleocene – mid Early Eocene) are distinguished in all sections by local or perhaps global and minor sea level transgression associated with early Eocene which was confirmed by (Speijer and Wagner, 2002; Baceta et al., 2011; Farouk 2016) and was identified by the change in microfacies' characteristics to the relatively more deep environments compared to the previous facies.

In the Aaliji Formation, the PETM zone revealed a slight increase in: matrix (clays and organic matter), clastic grains, radiolaria ratio (sea level rise), and dissolution porosity as well as paucity in benthic foraminifera especially after (sample A27) (Benthic Foraminifera Extinction Event (BFEE)) compared to pre PETM rocks Plate (2 a - d). Texturally, the facies exhibit dark greenish gray color mudstone and wackestone and sometimes wacke-packstone (sample A27) which may represent the (BFEE bed). Relatively, good sorting and increase in moldic vuggy porosity may be attributed to selective or normal dissolution.

In the Kolosh Formation, at Dohuk area, packages of petrographic features are noticed, where two calcarenite beds (sample D28, D31), perhaps representing (BFEE) and/

or LFT (Larger Foraminifera Turnover)) were deposited with the latest or end of Paleocene to early Eocene (between sample D28 to D32). These beds include bioclast fragments (large miscelanid nummulites, rotalides, less common milliolides, mollusca, bryozoa, bivalves, echinoderm and marine green algae (dasycladacean)), extraclasts, and rare lithoclasts (chert, quartz, feldspar and various rock fragments). The lithoclasts are less common than the bioclasts and all constituents merge in a micritic increasing up matrix, in addition to the magnetite or iron oxides which are arranged horizontally. These features relate to each other in a homogenous micritic matrix and vuggy to channel porosity and may be of a horizontal orientation texture, Plate (3 a, b, c). The Kolosh Formation in Shaqlawa area during the PETM zone has an increased magnetite (perhaps biogenic arranged in lamination or in a series or bullet-shaped), increased micritic or clay matrix (thick shale facies) (samples Q29, Q31), in contrast to other clastic grains, Plate (3 d - f).

Sea level rise hints were recorded and synchronized with the onset PETM stage environmental effects and continued during early Eocene. The rise was minor in the Aaliji Formation, (SMF 3) and continued in general, but the shifting basin ward took place from deep shelf/toe of slope contact environments to deep shelf /basin plain contact environments or (FZ2/FZ1). Because the (SMF3) facies emplaced in both FZ3 and FZ1 facies zones (Flügel, 2004), this small environmental shifting recognized by subfacies change within (SMF3) main facies when the wackstone dominance was replaced upward by a mudstone dominance in addition to the petrographic features mentioned previously.

In the Kolosh Formation at Shaqlawa section, the environmental perturbation was expressed by slowly finning up facies and an increase in calcareous blackish gray shale rather than thin marl. These changes were observed after (sample Q22) and the deepening petrographic features continued upward until the sandstone was revealed. The (SMF 3) with rare and small planktonic forams and more micritic organic matrix appeared in sample (Q29). All these phenomena indicate that environmental deepening or sea level rise was synchronized with PETM stage, thereby a minor shift occurred from (FZ3/FZ4) contact to the deepest end of (FZ 3) or from a slope/toe of the slope environment position (pre PETM) to near toe of slope /deep shelf interrelation environmental position (within outer ramp).

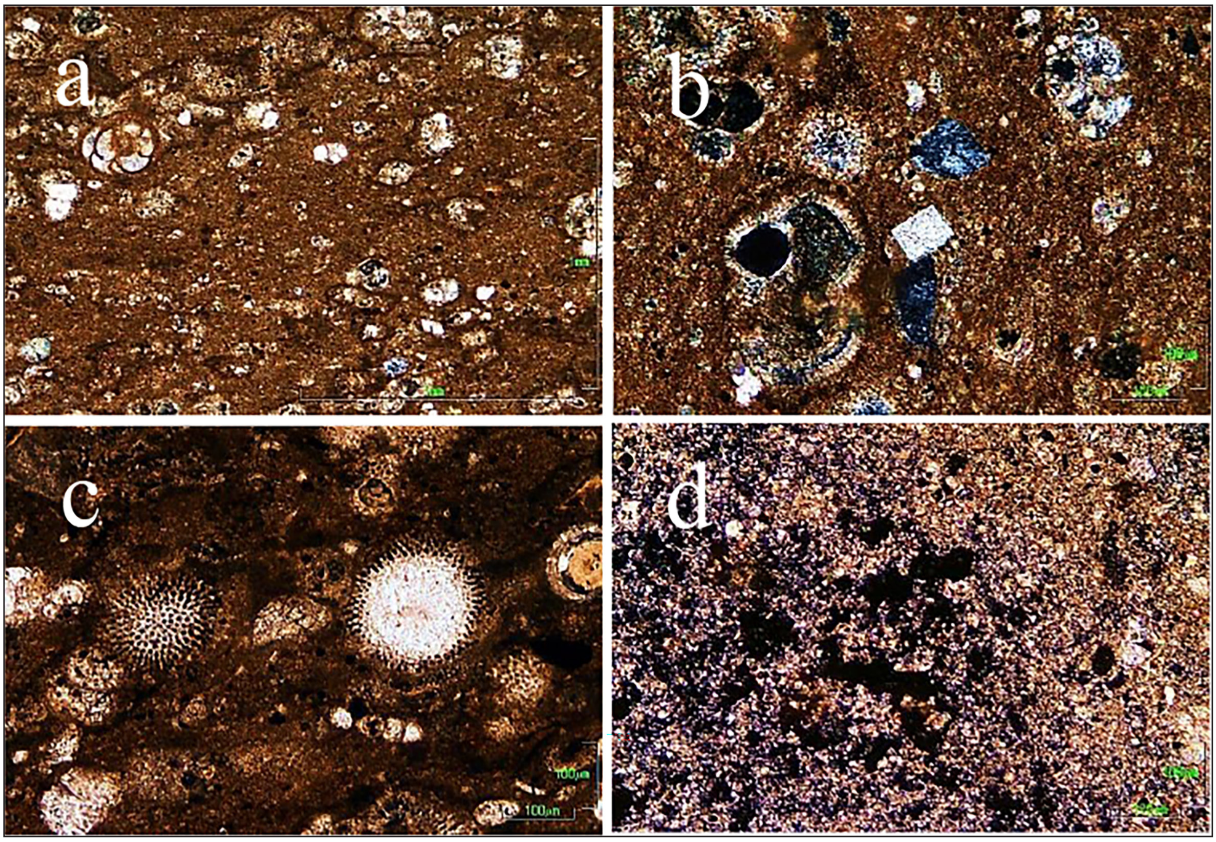

Plate 2. (a). Increasing in micritic or mud matrix (Sample A29). **(b).** Appearing clastic grains of quartz and chert with skeletal components (Sample A27). **(c).** Radiolaria skeletal grains, (Sample A29). **(d).** Spread in vuggy porosity due to dissolution or lysocline shallowing (Sample A24).

In the Kolosh Formation at the Dohuk section, the limited sea level rise make the facies (SMF5) in this stage spending more time within the deep parts of broad zone (FZ4). As sea level begins to rise, storm processes continue to rework and transport a skeletal material basin ward. Depletion of siliciclastics associated with transgression helps to concentrate or increase skeletal material at this time, and only a few large storms influence the deeper areas of the basin. Applying sequence stratigraphic terminology (Sageman, 1996), the packages correspond to lowstand and early transgressive system tracts. The vigorous hurricanes associated with global warming at subtropical platforms was enough to reach deeper areas of the basin slope (FZ4) forming two cycle of tempestite deposits, with the later one represented by (SMF 6) (sample D31). Generally, the PETM stage here is created in a slope or fore reef environment at or above the storm wave base level. However, the minor transgression observed clearly in this section may be attributed to the continuity forming a slope/ toe slope (mid/ outer ramp) environment at the end, especially when a turbidity character for the upper sandstone bed (sample D33) is obserevd. Although the finishing of the PETM tropical hurricanes effect gives a clue of the PETM decline, it does not necessarily mean the end of a minor transgression effect.

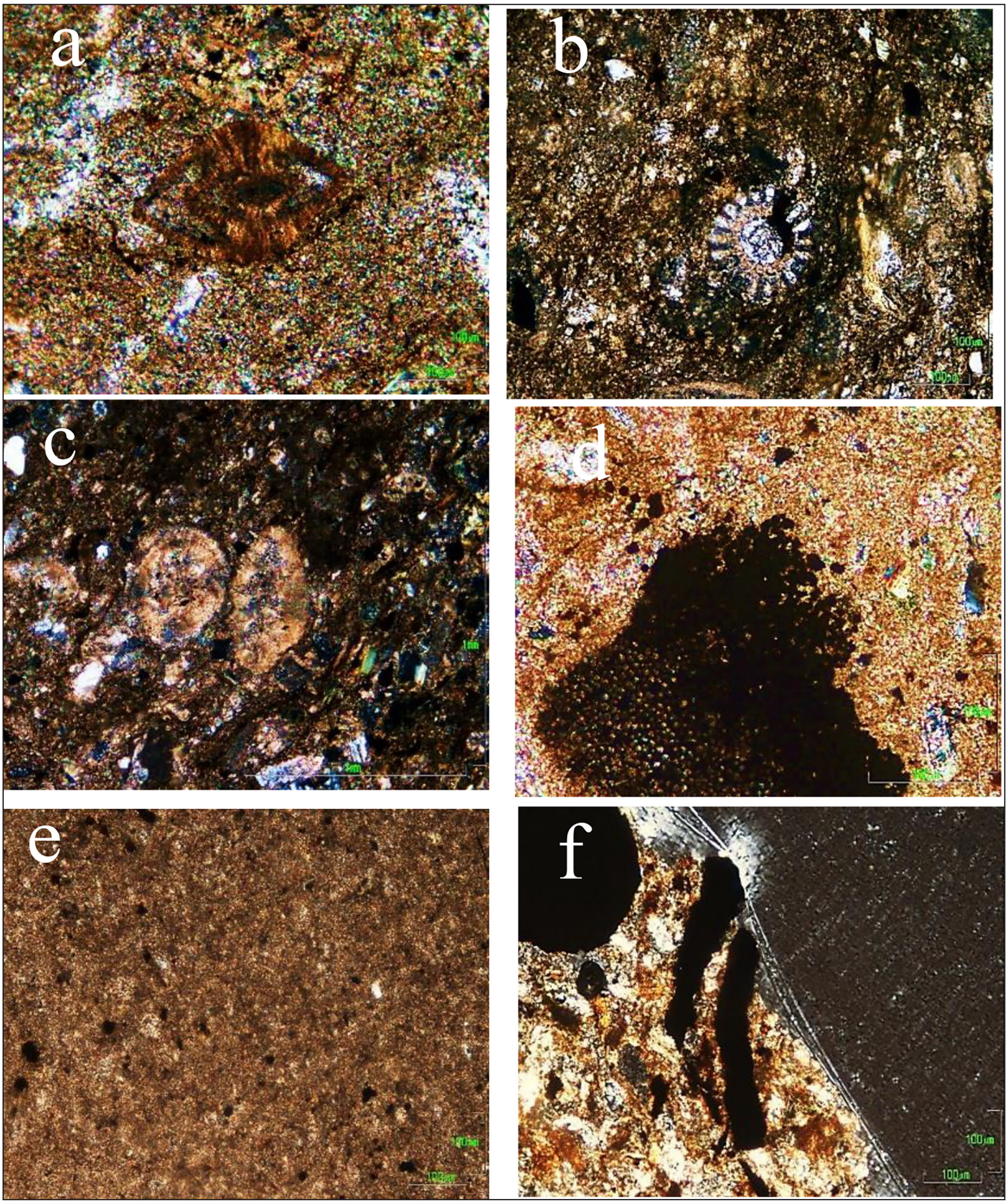

Plate 2. (a). Larger foraminifera Nummulites (Assilina) characterized by radial hyaline tests. Coiling is biconvex planispiral (Sample D28). **(b).** Blue green algal fragments(Dasycladacea) (SampleD29). **(c).** Decrease in clastic materials versus increase in bioclast and micritic matrix (Sample D28). **(d).** Common biogenic iron oxide crystals (Sample Q25). **(e).** Absence of clastic grains and the dominating micritic or mud matrix (Sample Q29). **(f).** Bullet-shaped and elongate chains of biogenic iron oxides (Sample Q27).

6.2 Clay Minerals

Since the Tertiary deposits' thickness within the Tethyan Sea did not exceed 1500 m, sediment did not suffer deep burial diagenesis, Therefore, clay minerals clues or imprint remained in the deposits (Bolle et al., 2000; Bolle and Adatte, 2001).

Generally, the clay mineral assemblages reflect the climatic conditions under which those minerals were weathered (Ghergari and Onac, 2001). Their relative abundance changes provide valuable information and good indicators about the prevailed climatic conditions such as warmness, aridity, humidity as well as the geoenvironmental conditions including the weathering rate.

XRD investigation has revealed that the following clay minerals are dominant in all of the studied sections; smectite (montmorillonite), illite, kaolinite, and palygorskite, Plate (4). The non-clay minerals are represented by calcite, ankerite, quartz, feldspar, hornblende, and rutile.

There are approximate shifts in clay values at the onset of early Eocene in all sections. In the Aaliji Formation, increases in all clay minerals as well as non- clay ankerite and quartz are recorded in Figure (13 A). In the Kolosh Formation at Dohuk section, the clay-mineral content fluctuates, which may refer to coastal perturbation, where an increase in illite, kaolinite and ankerite versus a decrease in quartz with a constant content in montmorillonite and an absence of palygorskite were observed Figure (13 B). In the Kolosh Formation at Shaqlawa section, there are very high increases in illite compared to montmorillonite, quartz and ankerite increase, conversely, there is a general decrease in kaolinite and paucity in palygorskite (0-0.3 wt. %), Figure (13 C).

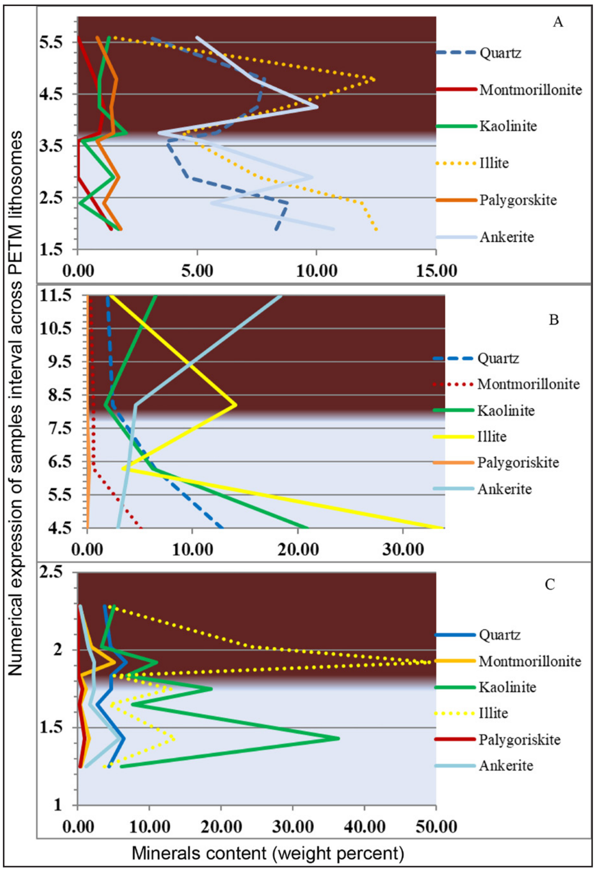

Figure 13. Distribution of clay minerals, Quartz, and Ankerite across the PETM lithosomes of the studied sections. **A.** Aaliji Formation. **B.** Kolosh Formation at the Dohuk section. **C.** Kolosh Formation at the Shaqlawa section, the contact between two colors correspond to the Paleocene / Eocene contact.

7. Discussion

7.1 PETM Geochemical Signatures

Many geochemical measures showed and separated the geochemical signatures that are used in singular or in integration with each other as an indication of environmental conditions that are characterized and associated with the PETM hyperthermal event.

In summary, the obtained geochemical signatures are the proven distinctive hints for carbon negative excursion (CIE), and the δ ^{18}O negative shifts are coincided with the early Eocene, and interpreted by the injection of huge amounts of 13C-depleted carbon into the ocean–atmosphere system, leading to an unusual temperature rise largely expressed by high oxygen (^{18}O) isotope negative peaks.

Major and trace-element analysis gives multi-indications of PETM, where the relative increase trend in most major oxides suggests a slight increase in contribution to the detrital materials (mostly clay minerals). On the other hand, the variations in the geochemical indices of paleoredox sensitive indicator ratios (for example; U/Th, U/Al and Mo/Al) indicate anoxic or euxinia conditions (Yao et al., 2018), while the increase in terrestrial input sensitive indicator ratios such as (Si/Al, K/Al, Zr/Al, Rb/Al) is a strong evidence of the progressive increase in the detrital input source with specific features. Other geochemical indices' variation such as (Ba/Al, Ti/Al, and Fe/Al provides more information about the environmental conditions such as productivity nature. Moreover, high terrestrial organic matter influx to the sea floor and improve its preservation as recorded in Teythan margins (including studied sections) evidenced by the high TOC concentration coordinated with anoxia, transient sea level rise, and the increase of primary productivity conditions.

Finally, the decrease in the $CaCO_3$ accumulation/preservation rates during the PETM was driven primarily by a significant increase in sea floor dissolution (lysocline shallowing) or are rather related to the siliciclastic dilution, while the lysocline deepening was signalled by increases in the $CaCO_3$ percentages (Alegret et al., 2018; Harper et al., 2019).

7.2 PETM Sedimentological Signals

In the Aaliji Formation, the increase in the radiolarian test reflects a good vertical water circulation (upwelling), and a decrease in $CaCO_3$ in the sediments because of the dissolution or CCD and the lysocline shallowing (Flügel, 2004 and 2010). Nevertheless, the increase in the dissolution porosity and the rarity of benthic foraminifera suggest the CCD and lysocline shallowing option as a global signal (Bralower et al., 2018), in addition to preparing for the upwelling process post PETM. The more micritic matrix and darker rock color observed in PETM zones were explained as a response to the sea level rise and high organic matter that may be associated with this high matrix (transient high productivity or eutrophy).

The calcareous tempestites in the Kolosh Formation are calcarenite at the Dohuk section and calcisiltite at the Shaqlawa section. The deposits are thought to be formed by tropical PETM-induced storms and hurricanes as is clear by the green algae (dasycladacean) (Flügel, 2004 and 2010). The presence of these calcareous tempestite shows that the deposition occurred below, but near to the storm wave base, and is mainly coincident with relative sea-level falls (lowstand) and early transgressive system tracts (TST) (Sageman, 1996). The rapid warming associated with the onset of the PETM caused significant changes in the environmental conditions (such as seasonality and high productivity); these variable environmental conditions would favour the diversification and proliferation of robust organisms adapted to exploit and tolerate periods.

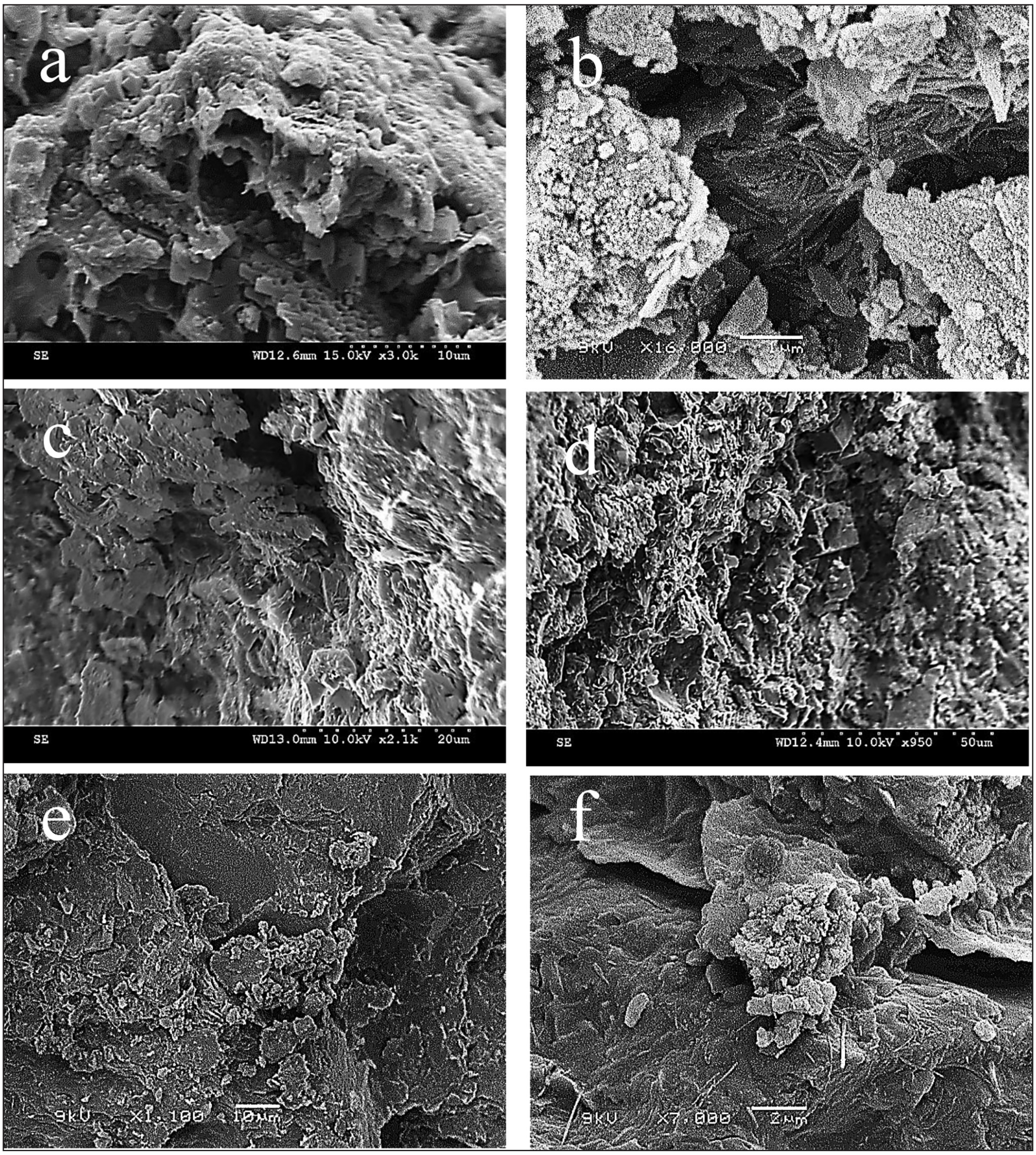

Plate 4. (a) Mostly authigenic montmorillonite (comb structure) (mo), detrital illite flakes (i) with dolomite rhombs (d). (A26). **(b)** Pore filling authigenic acicular palygorskite (p). (A27). **(c)** Spiny illite (i) coating grain or dolomite rhombs (arrows), vuggy micro porosity (mp) with detrital montmorillonite (mo). (D24). **(d)** Degraded illite flakes (arrows), dolomite rhombs partly dissolved (d), degraded kaolinite (k). (D28). **(e)** Degraded detrital kaolinite (k), highly degraded illite flakes (i) of detrital origin. (Q22). **(f)** Spiny palygorskite fibers (p) coating detrital framework grains, scattered carbonated (c). (Q24).

Magnetosomes of crystal shapes may be possibly identified in the Kolosh Formation, see Plate (2, f). They are typically arranged in elongate chains within the cell in order to direct the organism along the magnetic field lines and assist in the organism's search for nutrients. They might even be used as an intracellular energy or iron supply (Lippert, 2008). The environmental conditions spurred the magnetotactic bacteria bloom and the diversification of iron biomineralizing organisms specific to the subtropics in general, (they may also be global), although limited to the shallow continental shelves (Lippert, 2008; Rudmin et al., 2018) as noticed in Dohuk and some how at the Shaqlawa sections.

Vuggy – channel porosity observed in petrographic study could support the early dissolution idea or may be caused by synsedimentary to early diagenetic biogenic methane exhalation originating from the decay of organic matter (Liu et al., 1988 in Flügel, 2004). Both originating methods give a clue about the PETM event effect on sediment diagenesis.

The PETM abnormal paleoenvironmental conditions controlled the semi-consolidated PETM sediments' zone (early Eocene sediments) during its early diagenetic stage. Relative oxygen depletion or deficiency (not true anoxia), global increase in temperature, and the concentration of benthic food (eutrophic conditions) that prevailed within the sediments in the very shallow surface layer during the PETM show no record of trace fossil producers gradually but rapidly (Rodríguez-Tovar et al., 2011). This conclusion provides an indication of the weak or negligible effect of bioturbation diagenetic processes on the PETM zone sediments. However, the reduction condition and hypoxia are common along the Kolosh and Aaliji rocks, but increase during PETM zone as inferred by the increase of the pyrite authigenesis and TOC content (micritic matrix and dark color shale), absence of ichnofossils, and sediment lamination.

The PETM-induced sea level rise represents an indirect factor for the PETM impact, and possibly had a direct effect on the paleodepositional response, which resulted in originating the PETM depositional expression, tracing it through microfacies interpretation.

In the Aaliji Formation, although (SMF3) is dominated, the shifting basinward took place from deep shelf/toe of slope contact environments to deep shelf /basin plain contact environments. In the Kolosh Formation, at Shaqlawa section, minor shifts occurred from slope / toe of slope contact environments (per PETM) to near toe of slope /deep shelf interrelation. In the Kolosh Formation at Dohuk section, minor transgression was observed, from a slope or forereef environment to slope/ toe of slop transition environments especially when a turbidity character was observed upwards.

The climatic evolution of the Tethys in northern Iraq, as inferred by the clay mineralogy of the study areas had almost the same climatic trend as reported by Bolle and Adatte (2001) for southeastern Tethys. The coexisting of illite, smectite and some kaolinite indicate warm and seasonal (montmorillonite) climate fluctuating between humid (kaolinite) and dry (illite) episodes. This feature is confirmed by Wang et al. (2011) and Kemp et al. (2016). The presence of some authigenic palygorskite indicates an increase of hot conditions and aridity (Khormali et al., 2005).

The results revealed that detrital input is possibly the main source of kaolinite, smectite and illite, while in situ neoformation during the saline and alkaline environment this could be the dominant cause of palygorskite occurrences. Smaller amounts of kaolinite with the presence of smectite indicate the gradual shift to a more seasonal climate. From the late Paleocene to the early Eocene, the gradual decrease of kaolinite in low latitudes was coincident with gradual increases in illite, which indicates the progressive development of aridity and massive dryness and evaporation in the southeastern margins of Tethys (Bolle and Adatte, 2001).

The early Eocene samples are characterized by an increase in quartz grains in both of the Aaliji and Kolosh Formation at Shaqlawa section which is a function of a promoting increase in physical or mechanical weathering, erosion, and runoff. This is due to longer periods of aridity and probably foster less dense vegetation (e.g., Schmitz and Andreasson, 2001). Whereas, the increase of storm-induced tempestite as inferred by the recycled calcarenite beds' deposition explains the relatively detrital quartz-grain paucity in the Kolosh Formation at the Dohuk section Figure (13).

Kaolinite increased obviously at the Aaliji Formation as compared to the Kolosh Formation. The relative variations may be explained by the increasing of suspended kaolinite particles when transported from the nearshore resulting in differential accumulation settling at the offshore setting (Aaliji and occasionally in Kolosh Formation at Shaqlawa section) (Harding et al., 2011). The same cause may be attributed to the decreasing in montmorillonite in the Kolosh Formation at the Dohuk section Figure (13).

Both illite and ankerite increased in all the studied sections during the early Eocene Figure (13), which may suggest an increase in hydrothermal activities' weathering for illite in the source areas and hydrothermal deposition via early cementation or syndolomitization by ankerite; whereas Palygorskite developed and increased at the Aaliji Formation in addition some little increase at the Kolosh Shaqlawa section.

The increase in palygorskite is interpreted to be enhanced in arid, warm, and evaporative conditions, whereas the decreasing palygoriskite in the Kolosh Formation especially at the Dohuk section Figure (13) can be explained by the high terrigenous input, Mg-depletion due to syndolomitization or cementation, or by the Mg –transportation to a deeper sea position that inhibited the palygorskite formation in shallower environments.

7.3 PETM Environmental Scenario

7.3.1 Onset of the PETM

Stratigraphical, sedimentological, and geochemical signatures discussed in the previous sections characterize the onset of the PETM succession at Paleocene/Eocene boundary. The upper Paleocene relative sea-level fall or regression immediately preceding the PETM leads to the infilling of broad submarine channel or channel-like depressions (valley incision), causing erosion of the bordered exposed NW-SE ridge. This condition may be enhanced by earthquakes along major lestric faults (foreland basin) and, in shallow waters, by the effects of storm waves on the sea bed, and significantly induced terrigenous sediment input, gravity mass movement (slope failure), and completed a rapid progradation and/or upbuilding of extensive submarine fans (proximal to distal) that formed the Kolosh Formation deposits.

In addition to global/regional stimulates (e.g. volcanic activities), the Kolosh Formation depositional condition such as the decreasing pressure because slope masses failure and storm waves may largely have worked as a local inducer changing the stable methane clathrates' deposits, which are buried into older Aaliji and Kolosh semi consolidated deposits to unstable methane clathrates as an important source of carbon. The process of methane gas release is thus started increasingly. An input of huge amounts of isotopically light CO_2 and/or CH_4 into the earth system took place synchronizing with global PETM phenomena. Hence, warm climate takes to develop in northern Iraq region rapidly. Subsequently at the earliest Eocene, sea level started to rise responding to an early warming effect (melting of small ice sheets, sea water expansion or other agents) that is caused by the greenhouse gases' release and concurrent to the onset of deposition of the first PETM event beds or facies.

A progressive increase of weathering/ erosion rates and detrital (fluvial) input is strongly expected during the onset of the PETM as a normal environmental reaction to adjustment and the naturalized warming consequences. Increasing fluvial discharge prepared the sea water to developing primary saline water stratification as well as its thermal stratification. Water column stratification reduced vertical mixing or the upwelling process and immediately affected nutrient availability creating oligotrophic conditions (decrease productivity) with the onset of PETM (Alegret et al., 2018)

The onset of oxygen depletion in the deep sea may have occurred due to either the rapid oxidation of released methane from gas hydrates to carbon dioxide or the expansion and intensification of mostly terrestrial source organic matter zone, where the oxygen demand for the decay of metabolizable organic matter exceeds the rate of oxygen supply, Figures (14 A and B).

7.3.2 Peak phase of the PETM

The peak phase of PETM correspond to CIE peaks at the early Eocene time as the multi-sources release of greenhouse gases and global warming continued in a progressive manner. Certainly, this geologically rapid and chronic continuity affected the earth ecosystems, which responded through generating exceptional interplaying of environmental factors to contribute in the preparation of PETM environmental conditions. The inherent conditions from the onset of the PETM phase developed to become intemperate and severer in this phase.

The high concentration of greenhouse gases imposed excess amounts of CO_2 to be dissolved in marine ecosystems (as assumed in the studied sections paleoenvironment) to create an increase in H_2CO_3. Lowering in pH and $CaCO_3$ saturation (sea water acidification) (Babila et al., 2018), lysocline and CCD shallowing to naturalize acidification and widespread $CaCO_3$ dissolution took place severely reflecting leaching by corrosive waters. These changes were the most important factors in initiating the deposition of detrital clays within the early Eocene at the studied formations. On the other hand, increased temperatures, which intensified the hydrological cycle (Oliva-Urcia et al., 2018) resulted in an increase in humidity and hydrolysis reactions preparing for the next acceleration of weathering and erosion power rates which helped naturalize acidification through the increase of alkalinity as a result of dissolved bicarbonates supplied by fluvial discharge, then by lysocline deepening perhaps reaching its pre PETM original position.

Intense hydrological cycle is most likely associated with higher freshwater influxes that resulted in the establishment of density and /or salinity stratification (Frieling et al., 2018) in addition to weak thermal (low thermal gradient) stratification of the water column that led to extra water stratification and a high reduction in vertical circulation (upwelling) and horizontal circulation. Sea level rise may have shifted or expanded the upwelling regions towards shoreline areas (farther west Iraq) and consequently increased productivity in the photic zone, which also is more promoted by fluvial influx of organic / nutrients-rich sediments.

Relative enhancing in productivity by sea level rise and fluvial influxes, led to a more oxygen consumption within semi- stagnant water (good stratification). These parameters strongly supported the accumulation of organic carbon and promoted development of hypoxia or anoxia tendency state as explained by the presence of the lamination in deposits, and other previous indicators. The oxygen deficiency resulted in inhibited growth and elevated mortality prior to reaching the adult reproductive phase. Therefore, all PETM conditions particularly sea level rise and oxygen deficiency played an important role in restructuring the benthic ecosystem and benthic foraminifera extinction event (BFEE), immediately after the onset of global warming as in Figure (14 C).

7.3.3 The Recovery Phase of the PETM

Although a gradual transition exists between the PETM phase and the recovery phase (Lyons et al., 2019), its characteristic features were sensible after the early Eocene identified by the highest organic carbon (TOC) in concert with evidence and for oxygen-deficiency (such as lamination). The recovery phase was probably characterized by a rapid regrowth of terrestrial and marine organic inventories.

A number of negative feedback processes may have contributed to carbon sequestration including the expansion of continental vegetation with increased terrestrial organic carbon storage and/or elevated surface ocean productivity with increased marine organic carbon burial. Productivity enhancment likely originated through the development of more vigorous circulation due to the intensification of the wind. The enhanced vertical mixing was originatd by the upwelling of nutrient-rich intermediate Tethyan water into the epicontinental basin, and increase nutrient supply by fluvial discharge. However, quantitatively, the most important feedback for permanently sequestering carbon and lowering atmospheric CO_2 levels are the acceleration of silicate-weathering reactions on land.

The weathering mechanism would yield a net positive influx of bicarbonate and soluble cations into the ocean, thereby driving ocean carbonate content toward saturation and enhancing carbonate production/preservation rates until equilibrium was restored. An increase in the rate of carbonate sedimentation inferred by the increase of $CaCO_3$ percentage upward which would be consistent with the enhanced silicate weathering helped to promote a relatively rapid recovery from the CIE and falling global temperatures; the CO_2-triggered increased weathering and bioproductivity feedback effects possibly enhanced the subsequent progressive return to pre-PETM environmental conditions such as changing the waters to become progressively more oxic or (suboxia), Figure (14 D).

Finally, during the late recovery of the PETM, the siliciclastic flux has not returned to pre-event values, the concurrent sedimentary evidence for improved seafloor oxygenation, and excess in carbonate sedimentation considerably may reflect the lower siliciclastic input during a maximum flooding phase Figure (14 E).

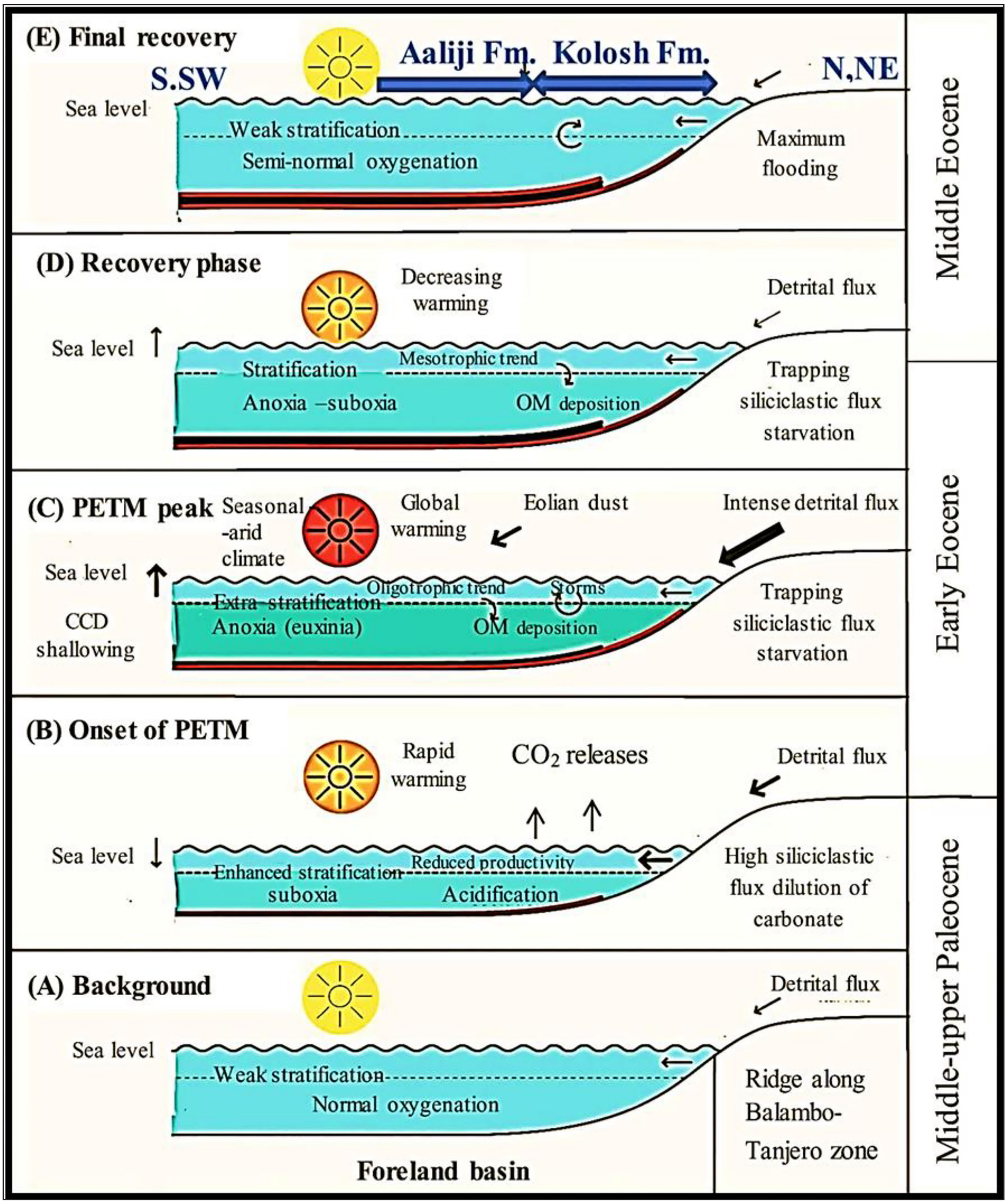

Figure 14. Conceptual model of climatic-environmental interplaying changes during the PETM event illustrated on an imagined paleogeographic cross section extending from N.NE to S.SW of Iraq. **(A).** Background conditions. **(B).** PETM onset. **(C).** PETM peak phase. **(D).** recovery phase, and **(E).** late recovery phase of this hyperthermal event. Modified after Schulte et al. (2011a).

8. Conclusions

1- The direct and indirect sedimentological, and geochemical indicators and the integration relationship among them suggest that during the Paleocene – early Eocene period, the northern Iraq region was affected by PETM climatic event interplayed in the marine realm within the epicontinental foreland basin. Both formations (Aaliji and Kolosh) are included at least in principle in the lithological or sedimentary records of PETM-associated events.

2- The fresh lithological color change to brown or yellowish brown or yellowish white colors is the distinctive field feature to trace the PETM equivalent lithosome in the Aaliji and Kolosh Formation outcrops as well as other field features such as the calciturbidite beds and /or organic matter rich black shale (deep marine) or calcarenitic tempestite beds (shallow marine).

3- There are several petrographic signals for the PETM environmental conditions identified in the Aaliji and Kolosh Formations such as magnetosomes (bacterial biomineralize), high matrix ratio, appearance of green algae (dasycladacean), as well as lack of bioturbation, early dissolution, and early dolomitization diagenetic process.

4- The PETM- related facies perturbations could be distinguished more obviously in shallow marine environments (Dohuk section) compared to deep marine environments (Aaliji Formation and Shaqlawa section).

5- A Paleoclimate trend (cold or warm) is an important and effective factor in facies model interpretations at least within minor sequence changes (smaller than third order).

6- Clay mineral assemblages and its variations across PETM lithosomes in the Aaliji and Kolosh Formations referred to same climatic trends of the southeastern Tethys region (warm, arid-seasonal climate).

7- The maximum flooding surface (MFS) is included within the PETM interval or lithosomes refering indirectly to the occurrence of transgressive system tracts (TST) associated with PETM effects.

8- The true carbon stable isotope values of sea water were represented more likely in The Kolosh Formation (Dohuk section) and the Aaliji Formation. In contrast, the original Oxygen stable isotope signal in the Aaliji Formation was less modified by diagenesis and was more preserved than in the Kolosh Formation.

9- The geochemical indices or ratios werea sensitive and a highly-valued method for tracing and identifying the anoxic or euxinia conditions and the rates of siliciclastic influx as well as the confirmation of other PETM-associated environmental factors such as the sea level rise and weathering intensity. Moreover, the variations in these ratios are, thus, considered the geochemical expression or responses of PETM-environmental interplaying.

10- The Kolosh Formation receives a siliciclastic flux with more extraneous material higher than the Aaliji Formation.

11- The increase of organic fluxes, increase of primary productivity, and improved preservation under anoxia conditions together caused the TOC enrichment during PETM at the studied sections.

References

Al Fattah, A. N., Al-Juboury, A.I., Ghafor, I. M. (in press). Biostratigraphic significance during the Paleocene-Eocene Thermal Maximum (PETM) in Northern and Northeastern Iraq.

Alegret L., Matíasc, R., Manuela, V. (2018). Environmental instability during the latest Paleocene at Zumaia (Basque-Cantabric Basin). The bellwether of the Paleocene-Eocene Thermal Maximum. Palaeogeography, Palaeoclimatology, Palaeoecology 497:186- 200.

Alegret, L., Ortiz S., Arenillas, I., Molina, E. (2010). What happens when the ocean is overheated? The foraminiferal response across the Paleocene–Eocene Thermal Maximum at the Alamedilla section (Spain). Geol. Soc. Am. Bull. 122:1616–24.

Al-Sharhan, A.S., and Nairn, A.E.M. (2003). Sedimentary basins and petroleum geology of the Middle East. Elsevier Science, Amsterdam, Netherlands P. 843.

Aqrawi, A.A.M., Goff, J.C., Horbury, A.D., Sadooni, F.N. (2010). The petroleum geology of Iraq, Scientific Press Ltd, UK, P.424.

Arthur, M.A., and Sageman, B.B. (2004). Sea-level control on source-rock development. Perspectives from the Holocene Black Sea, the Mid- Cretaceous Western Interior Basin on North America, and the Late Devonian Appalachian Basin. In. Harris, N. B. (Ed.), The Deposition of Organic-Carbon-Rich Sediments. Models, Mechanisms, and Consequences. SEPM Special Publication 82: 35–59.

Babila, T.L., Penman, D.E., Hönisch, B., Kelly, D.C., Bralower, T.J., Rosenthal, Y., Zachos, J.C. (2018). Capturing the global signature of surface ocean acidification during the Palaeocene–Eocene Thermal Maximum. Phil. Trans. R. Soc. A376.20170072. http.//dx.doi.org/10.1098/rsta.2017.0072.

Baceta, J., Pujalte, V., Wright, V.P., Schmitz, B. (2011): Carbonate platform models, sea-level changes and extreme climatic events during the Paleocene-early Eocene greenhouse interval: a basin- platform-coastal plain transect across the southern Pyrenean basin. In: Pree-Meeting Field trips Guidebook, 28th IAS Meeting. Zaragoza (C. Arenas, L. Pomar and F. Colombo, Eds.). Sociedad Geológica de España, Geo-Guías, 7:151-198.

Berggren, W.A., and Pearson, P.N. (2005). A revised tropical to subtropical planktonic foraminiferal zonation of the Eocene and Oligocene. Journal of foraminiferal Research 35: 279 – 298.

Bolle, M.P., and Adatte, T. (2001). Palaeocene–early Eocene climatic evolution in the Tethyan realm. clay mineral evidence. Clay Minerals 36: 249–261.

Bolle, M.P., Tantawy, A.A., Pardo, A., Adatte, T., Burns, S., Kassab, A. (2000). Climatic and environmental changes documented in the upper Paleocene to lower Eocene of Egypt. Eclogae Geologicae Helvetiae 93: 33–51 pp.

Bowen, G.J., Bralower, T.J., Delaney, M.L., Dickens, G.R., Kelly, D.C., Koch, P.L., Kump, L.R., Meng, J., Sloan, L. C., Thomas, E., Wing, S.L., Zachos, J.C. (2006). Eocene Hyperthermal Event Offers Insight Into Greenhouse Warming, EOS, Transactions of the American Geophysical Union 87: 165-169.

Bralower, T.J., Kump, L.R., Self-Trail, J.M., Robinson, M.M., Lyons, S., Babila, T., Ballaron, E., Freeman, K.H., Hajek, E., Rush, W., Zachos, C. (2018). Evidence for shelf acidification during the onset of the Paleocene-Eocene Thermal Maximum. Paleoceanography and Paleoclimatology33:1408-1426. https://doi.org/10.1029/2018PA003382.

Brasier, M.D. (1980). Microfossils. George Allen and Unwin Ltd., London, 193 p.

Cohen, A.S., Coe, A.L., Kemp, D.B. (2007). The Late Palaeocene-Early Eocene and Toarcian (Early Jurassic) carbon isotope excursions. a comparison of their timescales, associated environmental changes,causes and consequences. Journal of Geological Society London 164:1093—1108.

DeConto, R.M., Galeotti, S., Pagani, M., Tracy, D., Schaefer, K., Zhang, T., Pollard, D., Beerling, D.J. (2012). Past extreme warming events linked to massive carbon release from thawing permafrost. Nature 484, 87-91.

Dickens, G.R., O'Neil, J.R., Rea, D.K., Owen, R.M. (1995). Dissociation of oceanic methane hydrate as a cause of the carbon- isotope excursion at the end of the Paleocene, Paleoceanography, 10, 965–971.

Dickson, A.J., Cohen, A.S., Coe, A.L. (2012). Seawater oxygenation during the Paleocene-Eocene Thermal Maximum, Geology 40 (7): 639–642.

Dickson, A.J., Cohen, A.S., Coe, A.L. (2012). Geochemical facies analysis of fine- grained siliciclastics using Th/U, Zr/Rb and (Zr+Rb)/Sr ratios. Chemical Geology 181:131–146.

Elling, F.J., Gottschalk, J., Doeana, K.D., Kusch, S., Hurley, S.,J., Pearson, A. (2019). Archaeal lipid biomarker constraints on the Paleocene- Eocene carbon isotope excursion. NATURE COMMUNICATIONS (2019) 10.4519 | https.//doi.org/10.1038/s41467-019-12553-3.

Ernst, S.R., Guasti, E., Dupuis, CH., Speijer, R.P. (2006). Environmental perturbation in the southern Tethys across the Paleocene/Eocene boundary (Dababiya, Egypt). Foraminiferal and clay mineral records. Marine Micropaleontology 60: 89-111.

Farouk, S. (2016). Paleocene stratigraphy in Egypt. Journal of African Earth Sciences 113: 126-152.

Flügel, E. (2004). Microfacies of carbonate rocks, analysis, interpretation and application, Springer, Berlin P. 976.

Flügel, E. (2010). Microfacies of carbonate rocks, analysis, interpretation and application, 2nd edition, Springer, Berlin P. 984.

Fralick, P.W., and Kronberg, B.I. (1997). Geochemical discrimination of clastic sedimentary rock sources. Sedimentary Geology 113: 111– 124.

Frieling, J., Reichart, G. Middelburg, J. J., Röhl, U., Westerhold, T., Bohaty, S., M., Sluijs, A. (2018). Tropical Atlantic climate and ecosystem regime shifts during the Paleocene–Eocene Thermal Maximum. Clim. Past 14: 39–55. https.//doi.org/10.5194/cp-14-39- 2018.

Ghergari L. and Onac B. (2001). Late quaternary paleoclimate reconstruction based on clay minerals assemblage from preluca tiganului (gutai mountains, Romania), studia universitatis babes- bolyai, geologia, xlvi (1): 15-28.

Giusberti, L., Coccioni, R., Sprovieri, M., Tateo, F. (2009). Perturbation at the sea floor during the Paleocene–Eocene Thermal Maximum. Evidence from benthic foraminifera at Contessa Road, Italy. Marine Micropaleontology 70 (3–4): 102–119.

Giusberti, L., Rio, D., Agnini, C., Backman, J., Fornaciari, E., Tateo, F., Oddone, M. (2007). Mode and tempo of the Paleocene–Eocene Thermal Maximum in an expanded section from the Venetian pre- Alps. Geological Society of America Bulletin 119: 391–412.

Harding, I.C., Charles, A.J., Marshall, J.E.A., Pälike, H., Roberts, A.P., Wilson, P.A., Jarvis, E., Thorne, R., Morris, E., Moremon, R., Pearce, R.B., Akbari, S. (2011). Sea-level and salinity fluctuations during the Paleocene–Eocene thermal maximum in Arctic Spitsbergen, Earth and planetary Science Letters 303: 97- 107.

Harper, D.T., Hönisch, B., Zeebe, R., Shaffer, G., Haynes, L., Thomas, E., Zachos, J.,C. (2019). The magnitude of surface ocean acidification and carbon release during Eocene Thermal Maximum 2 (ETM-2) and the Paleocene–Eocene Thermal Maximum (PETM). Paleoceanography and Paleoclimatology https.//doi.org/10.1029/2019PA003699

Höntzsch, S., Scheibner, C., Guasti, E., Kuss, J., Marzouk, A.M., Rasser, M.W. (2011). Increasing restriction of the Egyptian shelf during the Early Eocene? — New insights from a southern Tethyan carbonate platform, Palaeogeography, Palaeoclimatology, Palaeoecology 302:349–366.

Hupp, B.N., Kelly, D.C., Zachos, J.C., Bralower, T.J. (2019). Effects of size- dependent sediment mixing on deep-sea records of the Paleocene- Eocene Thermal Maximum: Geology, v. 47, p. 749–752, https:// doi .org /10 .1130 /G46042.1.

Jassim, S.Z., and Buday, T. (2006). Middle Paleocene-Eocene Megasequence (AP 10). In Jassim, S.Z. and Goff, J.C. (Eds.). Geology of Iraq. Dolin, Prague and Moravian Museum, Brno, Czech Republic. P. 155-167.

John, C. M., Bohaty, S. M., Zachos, J. C., Sluijs, A., Gibbs, S., Brinkhuis, H., Bralower, T. J. (2008). North American continental margin records of the Paleocene–Eocene thermal maximum. Implications for global carbon and hydrological cycling. Paleoceanography 23, PA2217.

Jones, M.T., Percival, Stokke, E.W., Joost Frieling, J., Mather, T.A., Riber, L., Schubert, B.A., Schultz, B., Tegner, C., Planke, S., Svensen, H.H. (2019). Mercury anomalies across the Palaeocene–Eocene Thermal Maximum. Climate of the Past 15, 217-236, doi: 10.5194/cp-15-217- 2019.

Kemp, S.J., Ellis, M.A., Mounteney, I., Kender, S. (2016). Palaeoclimatic implications of highresolution clay mineral assemblages preceding and across the onset of the Palaeocene–Eocene Thermal Maximum, North Sea Basin. Clay Minerals 51: 793–813.

Kent, D.V., Cramer, B.S., Lanci, L., Wang, D., Wright, J.D., Van der Voo, R. (2003). A case for a comet impact trigger for the Paleocene/Eocene thermal maximum and carbon isotope excursion Earth Planet. Sci. Lett. 211 13– 26.

Khormali, F., Abtahi, A., Owliaie, H.R. (2005). Late Mesozoic-Cenozoic clay mineral successions of southern Iran and their paleoclimatic implications. Clay minerals 40: 191-203.

Khozyem, H., Adatte, T., Keller, G., Tantawy, A.A., Spangenberg, J.E. (2014). The Paleocene-Eocene GSSP at Dababiya, Egypt –Revisited. Episodes, 37 (2): 78-86.

Lipinski, M., Warning, B., Brumsack, H.J. (2003). Trace metal signatures of Jurassic/ Cretaceous black shales from the Norwegian Shelf and Barents Sea. Palaeogeography, Palaeoclimatology, Palaeoecology190: 459–475.

Lippert, P.C. (2008). Big discovery for biogenic magnetite, PNAS, 105, 46:17595-17596.

Lirer, F. (2000). A new technique for retrieving calcareous microfossils from lithified limedeposits. Micropaleontology 46: 365–369.

Liu, Q., Larrasoaña, J.C., Torrent, J., Roberts, A.P., Rohling, E. J., Liu, Z., Jiang, Z. (2012). New constraints on climate forcing and variability in the circum-Mediterranean region from magnetic and geochemical observations of sapropels S1, S5 and S6. Palaeogeography, Palaeoclimatology, Palaeoecology 333-334: 1–12.

Liu, Y.G., Miah, M.R.U., Schmitt, R.A. (1988). Cerium: Achemical tracer for paleo-oceanic redox conditions. Geochimica et Cosmochimica Acta 52 (6): 1361-1371

Lyons, S.L., Baczynski, A. A., Babila,T.L., Bralower, T.J., Hajek, E.A., Kump, L. R., Polites, E.G., Self-Trail, J.M.,Trampush, S.M., Vornlocher, J.R., Zachos, J.C., Freeman, K.H. (2019). Palaeocene– Eocene Thermal Maximum prolonged by fossil carbon oxidation. Nature Geosc ience 12 (1): 54–60. https://hdl.handle.net/10.1038/s41561- 018 0277-3

Mazzullo, S.J. (2000). Organogenic dolomitization in peritidal to deep-sea sediments. Journal of Sedimentary Research 70 (1): 10-23.

Meadows, D.J. (2008). Geochemistry of the Paleocene Tartan Formation in the Great South Basin, New Zealand, Unpublished Diploma Thesis, Victoria University of Wellington, P.108.

Nguyen, T.M.P., Petrizzo, M.R., Speijer, R.P. (2009). Experimental dissolution of a fossil foraminiferal assemblage (Paleocene–Eocene Thermal Maximum, Dababiya, Egypt). Implications for paleoenvironmental reconstructions. Marine Micropaleontology 73:241–258.

Nicolo, M.J., Dickens, G.R., Hollis, C.J., Zachos, J.C. (2007). Multiple Early Eocene hyperthermals. Their sedimentary expression on the New Zealand continental margin and in the deep sea. Geology 35: 699- 702.

Oliva-Urcia, B., Gil-Peña, I., Samsó, J.M., Soto, R., Rosales, I. (2018). A Paleomagnetic Inspection of the Paleocene-Eocene Thermal Maximum (PETM) in the Southern Pyrenees. Front.

Earth Sci. 6:202. Doi: 10.3389/feart.2018.00202.

Rodríguez-Tovar, F.J., Uchman A., Alegret, L., Molina, E., (2011). Impact of the Paleocene–Eocene Thermal Maximum on the macrobenthic community. Ichnological record from the Zumaia section, northern Spain, Marine Geology 282: 178–187.

Röhl, U., Westerhold, T., Bralower, T.J., Zachos, J.C. (2007). On the duration the Paleocene–Eocene Thermal Maximum (PETM). Geochemistry, Geophysics, Geosystems 8 (12): 1-13.

Rudmin, M., Roberts, A.P., Horng, C.S., Mazurov, A., Savinova, O., Ruban, A., Veklich, M. (2018). Ferrimagnetic iron sulfide formation and methane venting across the Paleocene-Eocene thermal maximum in shallow marine sediments, ancient West Siberian Sea. Geochemistry, Geophysics, Geosystems19: 21–42. https://doi.org/10.1002/2017GC007208.

Sageman, B.B. (1996). Lowst and tempestites. Depositional model for Cretaceous skeletal limestones, Western Interior basin, Geology 24 (10): 888–892.

Schaller, M.F., Fung, M.K., Wright, J.D., Katz, M.E., Kent, D.V. (2016). Impact ejecta at the Paleocene-Eocene boundary Science 354: 225–9.

Scheibner, C. and Speijer, R.P. (2008). Late Paleocene–early Eocene Tethyan carbonate platform evolution — a response to long- and short-term paleoclimatic change. Earth-Science Reviews 90: 71– 102.

Schmitz, B., and Andreasson, F.P. (2001). Air humidity and Lake δ18O during the latest Paleocene–earliest Eocene in France from recent and fossil fresh-water and marine gastropod δ18O, δ13C, and 87Sr/86Sr. Bulletin of the Geological Society of America 113: 774– 789.

Schmitz, B., Asaro, F., Molina, E., Monechi, S., Von Salis, K., Speijer, R. (1997). High-resolution iridium, δ13C, δ18O, foraminifera and nannofossil profiles across the latest Paleocene benthic extinction event at Zumaya, Spain. Palaeogeography, Palaeoclimatology, Palaeoecology 133: 49–68.

Schmitz, B., Peucker-Ehrenbrink, B., Heilmann-Clausen, C., Aberg, G., Asaro, F., Lee, C. T. A. (2004). Basaltic explosive volcanism, but no comet impact, at the Paleocene–Eocene boundary. High-resolution chemical and isotopic records from Egypt, Spain and Denmark. Earth and Planetary Science Letter 225: 1–17.

Schulte, P., Joachim, C., Brumsack, H., Mutterlose, J. (2011b). Element chemostratigraphy across the Paleocene-Eocene thermal maximum at Demerara Rise, Central Atlantic (ABSTRACT), Berichte Geol. B. - A., 85 (ISSN 1017-8880)– CBEP 2011, Salzburg, June 5th – 8th.

Schulte, P., Scheibner, C., Speijer, R. (2011a). Fluvial discharge and sea- level changes controlling black shale deposition during the Paleocene–Eocene Thermal Maximum in the Dababiya Quarry Section, Egypt. Chem. Geol. 285: 167– 183.

Sharland, P.R., Archer, R., Casey, D. M., Davis, R.B., Hall, S.H., Heward, A.P., Horbury, A.D., Simmons, M.D. (2001). Arabian Plate Sequence Stratigraphy. GeoArabia, Special publication, no. 2. P. 372.

Sluijs, A., Bowen, G. J., Brinkhuis, H., Lourens, L.J., Thomas, E., (2007). The Palaeocene-Eocene thermal maximum super greenhouse. Biotic and geochemical signatures, age models and mechanisms of global change. In. M. Williams, et al. (Eds.) Deep time perspectives on Climate Change. Marrying the Signal from Computer Models and Biological Proxies. The Micropalaeontological Society, Special Publications, the Geological Society, London, 323-349.

Sluijs, A., Röhl, U., Schouten, S., Brumsach, H.J., Sangiorgi, F., Sinninghe Damsté, J.S., Brinkhuis, H. (2008). Arctic late Paleocene–early Eocene paleoenvironments with special emphasis on the Paleocene – Eocene thermal maximum (Lomonosov Ridge, Integrated Ocean Drilling Program Expedition 302). Paleoceanography 23, PA1S11. Doi:10.1029/2007PA001495.

Soliman, M.F., Aubry, M.P., Schmitz, B., Sherrell, R.M. (2011). Enhanced coastal paleoproductivity and nutrient supply in Upper Egypt during the Paleocene/Eocene Thermal Maximum (PETM). Mineralogical and geochemical evidence, Palaeogeography, Palaeoclimatology, Palaeoecology 310: 365–377.

Speijer, R., and Wagner, T. (2002). Sea-level changes and black shales associated with the late Paleocene thermal maximum. Organic- geochemical and micropaleontologic evidence from the southern Tethyan margin (Egypt-Israel). Boulder. Geological Society of America, Special Paper 356: 533-549.

Svensen, H.S., Planke, A., Malthe-Sorenssen, B., Jamtveit, R., Myklebust, T., Eidem, S.R. (2004). Release of methane from a volcanic basin as a mechanism for initial Eocene global warming, Nature 429: 542-545.

Thomas, D.J., and Bralower, T.J. (2005). Sedimentary trace element constraints on the role of North Atlantic Igneous Province volcanism in late Paleocene–early Eocene environmental change. Marine Geology 217: 233–254.

Tremolada, F., and Bralower, T.J. (2004). Nannofossil assemblage fluctuations during the Paleocene–Eocene Thermal Maximum at Sites 213 (Indian Ocean) and 401 (North Atlantic Ocean). Palaeoceanographic implications. Marine Micropaleontology 52: 107– 116.

Uchikawa, J., and Zeebe, R.E. (2010). Examining possible effects of seawater pH decline on foraminiferal stable isotopes during the Paleocene–Eocene thermal maximum. Paleoceanography 25, PA2216. doi:10.1029/2009PA001864

Veizer, J. (2009). Carbon Isotope Variations over Geologic Time, in Gornitz, V. (Ed). Encyclopedia of Paleoclimatology and Ancient Environments, Springer P. 1047.

VVer Straeten, C.A., Brett, C.E., Sageman, B.B. (2011). Mud rock sequence stratigraphy.Amulti-proxy (sedimentological, paleobiological and geochemical) approach, Devonian Appalachian Basin, Palaeogeography, Palaeoclimatology, Palaeoecology 304: 54–73.

Wang, C.W., Hong, H.L., Song, B.W., Yin, K., Li, Z.H., Zhang, K.X.,J.I. J.L. (2011). The early-Eocene climate optimum (EECO) event in the Qaidam basin, northwest China. Clay evidence. Clay Minerals 46: 649–661.

Yao, W., Paytan, A., Wortmann, U.G. (2018). Large-scale ocean deoxygenation during the Paleocene-Eocene Thermal Maximum. Science, 361: 804-806.

Zachos, J. C., Röhl, U., Schellenberg, S. A., Sluijs, A., Hodell, D. A., Kelly, D. C., Thomas, E., Nicolo, M., Raffi, I., Lourens, L. J., McCarren, H., Kroon, D. (2005). Rapid Acidification of the Ocean during the Paleocene-Eocene Thermal Maximum, Science 308 (5728): 1611- 1615.

Zachos,J.C., Lohmann, K.C., Walker, J.C.G., Wise, S.W. (1993). Abrupt Climate Change and Transient Climates during the Paleogene: A Marine Perspective. The Journal of Geology 101(2):191-213, DOI: 10.1086/648216.

Zeebe, R.E. (2013) What caused the long duration of the Paleocene-Eocene Thermal Maximum? Paleoceanography 28, 440-452.

Zeebe, R.E., and Lourens, L.J. (2019). Solar System chaos and the Paleocene–Eocene boundary age constrained by geology and astronomy. Science 365: 926–929.

Zhang, Q., Dinga, L., Kitajimac, K., Valleyc, J.W., Zhangd, B., Xua, X., Willems, H., Klügelb, A. (2019). Constraining the magnitude of the carbon isotope excursion during the Paleocene-Eocene thermal maximum using larger benthic foraminifera. Global and Planetary Change 184 (2020) 103049.